THESIS

FIRE AND ICE: ANALYZING ICE NUCLEATING PARTICLE EMISSIONS FROM WESTERN U.S. WILDFIRES

Submitted by

Kevin Robert Barry

Department of Atmospheric Science

In partial fulfillment of the requirements

For the Degree of Master of Science

Colorado State University

Fort Collins, Colorado

Fall 2019

Master's Committee:

Advisor: Sonia Kreidenweis
Co-Advisor: Paul DeMott

Elizabeth Barnes
Delphine Farmer

ABSTRACT

FIRE AND ICE: ANALYZING ICE NUCLEATING PARTICLE EMISSIONS FROM WESTERN U.S. WILDFIRES

Wildfires in the western U.S. can have impacts on health and air quality and are forecasted to increase in the future. Some of the particles released from wildfires can affect cloud formation through serving as ice nucleating particles (INPs). INPs are necessary for heterogenous ice formation in mixed-phase clouds at temperatures warmer than about -38 °C and can have climate implications from radiative impacts on cloud phase and by affecting cloud lifetime. Wildfires have been shown to be a potential source of INPs from previous ground-based measurement studies, but almost no data exist at the free tropospheric level that is relevant for cloud formation. The Western Wildfire Experiment for Cloud Chemistry, Aerosol Absorption, and Nitrogen (WE-CAN) campaign that was conducted in summer 2018 utilized the NSF/NCAR C-130 to sample many smoke plumes of various ages in the free troposphere and aged smoke in the boundary layer. INP measurements were made with the CSU Continuous Flow Diffusion Chamber (CFDC) and with aerosol filter collections to analyze offline with the CSU Ice Spectrometer (IS). The results presented in this thesis indicate a contribution of smoke to the INP number concentration budget over the plume-background air, but much variability exists in concentrations and in INP composition among fires. Treatments of the filter suspensions show a dominant organic influence in all plume filters analyzed while a biological INP population is evident in several cases. For the South Sugarloaf fire, which had a primary fuel of sagebrush shrubland, the highest INP concentrations of the campaign were measured, and

the unique INP temperature spectrum suggests lofting of material from uncombusted plant material. Normalization of INP concentrations measured in WE-CAN confirms that smoke is not an especially efficient source of ice nucleating particles, however emissions impacts may still occur regionally. The determination of a Normalized Excess Mixing Ratio (NEMR) of INP emissions for the first time will permit modeling of such impacts, and possible INP in-plume production will be explored in future research.

ACKNOWLEDGEMENTS

I would like to thank my advisors, Dr. Sonia Kreidenweis and Dr. Paul DeMott, for their continual support in helping me develop as a researcher. It has been an honor to learn from two very accomplished scientists and they have been great mentors. I would like to thank Dr. Thomas Hill as being an invaluable part to this research and also to me as a student, from instrument training and strategy to interpretation of results. Dr. Ezra Levin and Kathryn Moore have been helpful in my first field campaign experience, and Dr. Emily Fischer and the rest of the WE-CAN team have been great to work with. I would lastly like to thank the rest of my master's committee, Dr. Elizabeth Barnes and Dr. Delphine Farmer, for useful feedback and discussions that helped me see my research questions from multiple perspectives.

TABLE OF CONTENTS

1. Introduction

1.1. Importance of Wildfires as a Source of Particles to the Atmosphere

Wildfires are a known human health hazard that can have significant atmospheric impacts across the world and can severely impact air quality (Figure 1.1). This thesis focuses on measurements from wildfires in the Western U.S. They are a large source of particulate matter having diameters smaller than 2.5 μm ($PM_{2.5}$). U.S. trends of $PM_{2.5}$ in the 98^{th} quartile are all negative except in the Northwestern U.S., which is likely due to wildfires offsetting improvements in lowering emissions of anthropogenic pollutants (McClure and Jaffe, 2018). Western U.S. wildfires are forecasted to increase in the future, as suggested by Westerling et al. (2016), who also found an increase in the frequency of large wildfires (more than 400 hectares) in each decade since the 1970s. There have also been increases in fuel aridity in the western U.S. forest fire areas over the past few decades along with longer fire seasons (Abatzoglou et al., 2016). The particles released from wildfires can have an effect on climate through their scattering and absorbing properties and may also affect cloud and precipitation formation through serving as cloud condensation nuclei (CCN) or as ice nucleating particles (INPs).

Figure 1.1. Example of wildfire smoke affecting regional air quality at Boise Airport in summer 2018. Photos are separated by 5 days. Photo by Kevin Barry.

1.2. Aerosol-cloud Interactions in Cold Clouds and Climate Impacts

Here, we focus on the possible interactions of particles emitted in wildfires with clouds, and especially for clouds forming at temperatures colder than 0 ˚C. In the atmosphere, cloud droplets remain supercooled until about -38 °C, which is the homogeneous freezing temperature of cloud droplet-sized volumes of pure water. However, when some types of INPs are present as cloud droplets, the droplets are able to freeze heterogeneously at much warmer temperatures below 0 °C. This immersion freezing process (Vali et al., 2015) is thought to be the dominant heterogeneous ice nucleation mechanism globally (Section 1.3). Outside of the tropics, where warm rain (i.e., from clouds entirely in the liquid phase) dominates, precipitation is largely controlled by the formation of rain or snow in ice- and mixed-phase clouds (Mülmenstädt et al., 2015). Since temperatures between 0 and -38 °C are relevant for mixed-

phase clouds, INPs therefore have an important effect on precipitation initiation. However, INPs are very rare, as for example, Rogers et al. (2001) measured a median of 20 INPs out of 1,000,000 total particles for a median activation temperature of -20 °C during eight research flights over the Arctic Ocean. Although the abundance of INPs changes seasonally, with location, and with freezing temperature, total aerosol number concentration is always in great excess with respect to INPs. Within specific aerosol types or categories, such as mineral dusts and sea salt, the proportion of the population active as INPs at a particular temperature depends on the ice nucleation efficiency, as discussed in Section 1.4.

The altitude of a cloud in the atmosphere has large ramifications for climate, especially concerning the impacts of changes in aerosol properties feeding clouds. Clouds at all heights effectively reflect sunlight, considered a cooling effect, but high clouds reduce the top of atmosphere (TOA) outgoing longwave radiation by emitting at much colder temperatures in the upper troposphere so increases in abundance would have a warming effect (Lohmann and Gasparini, 2017). Conversely, lower and mid-level clouds emit at higher temperatures (closer to the warmer surface) and thus do not affect the TOA outgoing longwave radiation as much, so they generally exert a cooling effect. INPs can have an effect on cloud radiative properties and on cloud lifetimes of midlevel and high clouds, and therefore impact the climate in complex ways. Their modes of impact have been previously referred to as the ice indirect effect (Lohmann et al., 2002), as discussed in DeMott et al. (2010) (Figure 1.2). More INPs in midlevel clouds (temperatures between -5 and -30 °C) may lead to greater precipitation from enhanced ice crystal concentrations and thereby lead to shorter cloud lifetimes and a reduction of the cooling effect. An increase in INPs in high cirrus clouds may reduce the warming effect by from

competition with homogeneous freezing and subsequently reducing the cloud lifetimes from sedimentation. However, since cirrus clouds under the enhanced-INP scenario would likely cover larger areas due to ice forming at lower relative humidity, the net impact for a given INP scenario is more difficult to predict without detailed numerical simulations. Likewise, if INP concentrations are reduced, this could lead to longer mid- and high-level cloud lifetimes and amplifications in the cooling and warming effects respectively. Moreover, ice crystals and water droplets at the same size can have quite different radiative properties (Figure 1.3). The single scatter albedo quantifies the fraction of radiation scattered to extinguished (scattered plus absorbed) and varies as a function of wavelength. These contrasts clearly show that cloud phase has a strong impact on cloud radiative properties and the differences are also useful for distinguishing between ice and water in satellite retrievals. Due to the potentially significant climate impacts of INPs, efforts have been made to measure and model INP sources and atmospheric concentrations as well as further understanding of the mechanisms of ice nucleation.

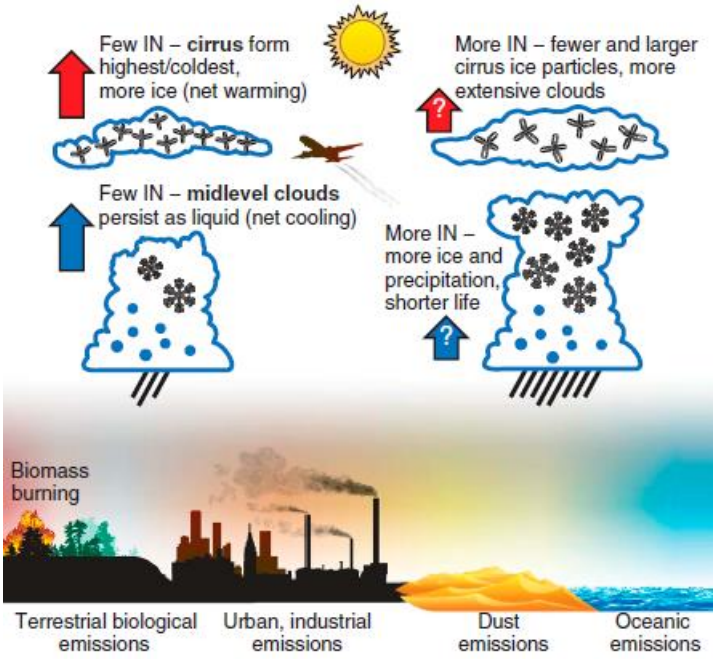

Figure 1.2. The ice indirect effect from DeMott et. al (2010), Figure 1, showing potential INP sources and the uncertainty in the cooling and warming impacts of midlevel and high clouds respectively with changing INP concentrations.

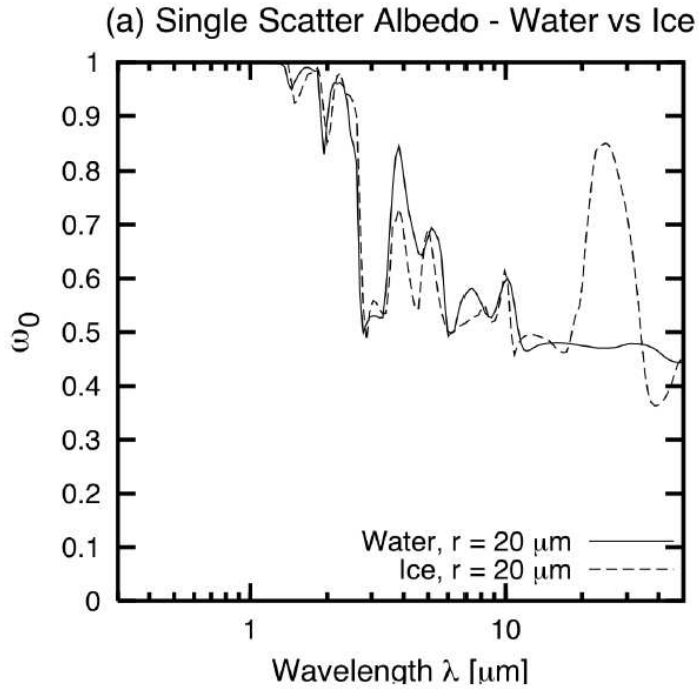

Figure 1.3. The single scatter albedo for ice and water droplets as a function of wavelength. Figure is from Petty 2006, 12.10a.

1.3. Heterogeneous Nucleation of Ice and Prior Work on INP Characterization

Heterogeneous ice nucleation can proceed by deposition ice nucleation, where water vapor is supersaturated with respect to ice and thought to condense as ice directly onto an INP; contact freezing, where an INP collides with a droplet that subsequently freezes; or by immersion/condensation freezing, where an INP is immersed in a water droplet that supercools and initiates freezing at some temperature below 0 °C (Vali et al., 2015). Murray et al. (2012) discuss evidence for the importance of liquid as a prerequisite for formation of ice in mixed-phase clouds (e.g. de Boer et al., 2011), and measurements in this thesis are primarily considered in the immersion freezing mode.

Increasing numbers of campaigns are occurring around the globe to characterize the sources and concentrations of INPs. Many particle types have been shown in the laboratory and in observational studies to serve as INPs at atmospheric conditions, including dust, organics, volcanic ash, metals, and biological material (Kanji et al., 2017). Among terrestrial sources (i.e., non-marine), mineral dust has been consistently shown to be a dominant fraction of the number concentration of INPs active at temperatures above the homogeneous freezing limit, arising from long-range transport of deserts dusts that can lead to elevated INP concentrations far from the source (DeMott et al., 2003). Pratt et al. (2009) quantified that mineral dust comprised approximately 50 percent of ice crystal residuals in clouds sampled over Wyoming. Mineral dust is most important at the lower temperature end of the mixed-phase regime and is not expected to represent a large contribution to the budget of INPs warmer than about -15 °C or -10 °C (Price et al., 2018; DeMott et al., 2015; Murray et al., 2012).

Organic aerosols are also known to play a role as INPs, although this category is the most poorly understood and quantified for the atmosphere. The category includes both purely biological particles and unidentified organic compounds. Bacteria and eukaryotes like fungi, plant tissue, lichens, and pollen have all been identified as INP sources, with some initiating ice at temperatures as warm as -5 °C (Hill et al., 2018). Specific sources of biological INPs have been previously reported for the Western U.S., the focus region for this study. Bowers et al. (2011) estimated biological INP concentrations over agricultural, forest, and suburban land areas in northern Colorado and found that agricultural lands were the largest source of INPs (up to eight times higher than other areas analyzed) on the basis of assuming a biological source only for particles active at temperatures warmer than -10°C . Suski et al. (2018) investigated INP emissions during the harvesting season (e.g. from soil dust and plant fragments) in the Great Plains and saw a significant contribution of INPs that were active over a broad temperature range and heat-labile (and therefore likely biological), along with finding the presence of (non-specific) ice nucleating bacteria. Known ice nucleating bacteria have also been identified in emissions from harvesting over this region (Hill et al., 2018). Soils tested in Wyoming and Colorado also showed a large organic INP presence (Tobo et al., 2014; Hill et al., 2016), although biological types within soil particles dominated progressively only at temperatures warmer than -12 °C and other more stable organic types comprised over 90% of soil INPs over a temperature range to as low as -30 °C. However, the air and ground can have extensive variation in INPs, and mechanisms of emission are also poorly understood. For example, measurements from vegetation at a Colorado farm indicated the presence of ice nucleation-active (INA) bacteria that were up to 2 x 10^7 per gram of vegetation but were at the detection

limit of INPs in air (Garcia et al., 2012). Hill et al. (2014) also found low amounts of INA bacteria in several precipitation samples, although there was still a large unidentified labile biological component on the basis of their sensitivity to destruction after heating to 95 °C.

1.4. Biomass Burning as a Source of INP

Wildfires are a potential INP source, presenting a ready means for lofting large mass concentrations of carbonaceous and other types of aerosols, but as shown in Figure 1.4 in red, have limited field measurements. INP measurements have been made from a large number of plant fuels in laboratory studies over many years. In the FLAME 2 study in Missoula, Montana, 21 different fuels were tested that are characteristic of wildfires and prescribed burns in the U.S. (Petters et al., 2009). Many of the tests did not produce detectable numbers of INPs active at -30 ˚C. Swamp sawgrass smoke was the most consistent source for repeated burns and had the highest ice nucleation efficiency parameter (Figure 1.5). This parameter describes the activated fraction of INPs (i.e., INP concentrations divided by the total particle concentration at a given temperature). Figure 1.5 also shows other fuels that served as potential sources of INPs in those experiments. Petters et al. (2009) estimated that if INPs represent greater than 1 out of 10,000 particles emitted in smoke, they can have regional impacts on the INP budget (from a bottom-up emissions approach). They also indicated that the fuels producing the highest number fractions of INPs were associated with higher potassium, nitrate, and inorganic fractions as well as higher hygroscopicity and lower organic carbon fraction. In the FLAME 4 study, Levin et al. (2016) repeated laboratory measurements of some of the same fuels, added others, derived INP emission factors based on the amount of fuel consumed, and explored the role of soot-containing particles as potential INPs (most measurements made at -30 °C). A

similar proportion of fuels were found to be INP sources as found by Petters et al. (2009), but the ice nucleation efficiency factors were generally more variable and lower. Overall, Levin et al. (2016) showed that fires can be an important source of heterogeneous ice nuclei in terms of their contributions to ambient INP concentrations in the free troposphere, although the ice nucleation efficiencies are lower than other known INP types and rarely meet the criteria stated by Petters et al. (2009) for regional importance.

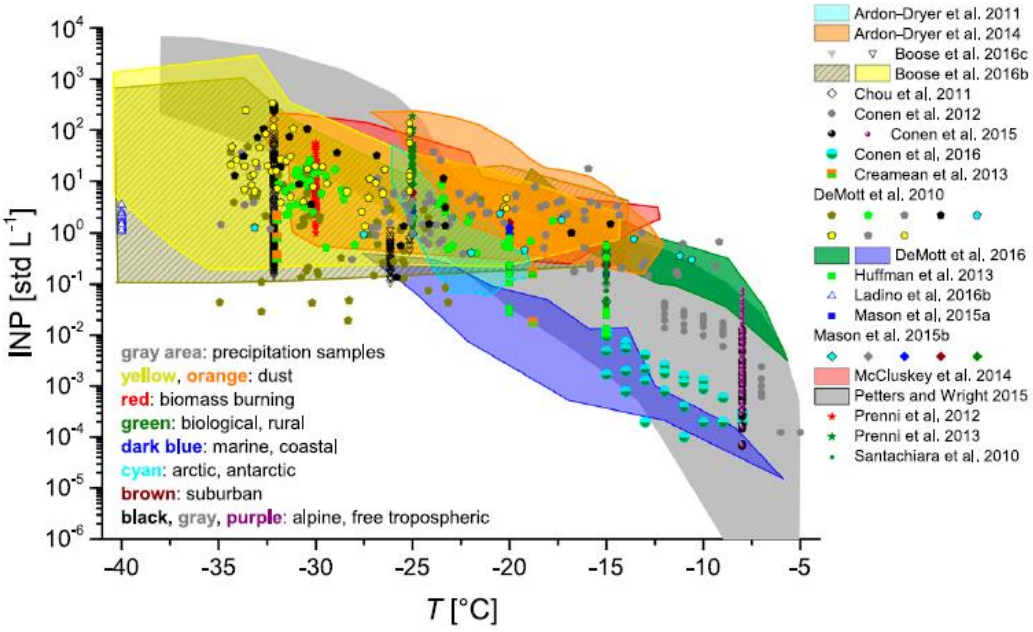

Figure 1.4. Field measurements of INP concentrations, colored by INP type. From Kanji et al. 2017, Figure 1-10.

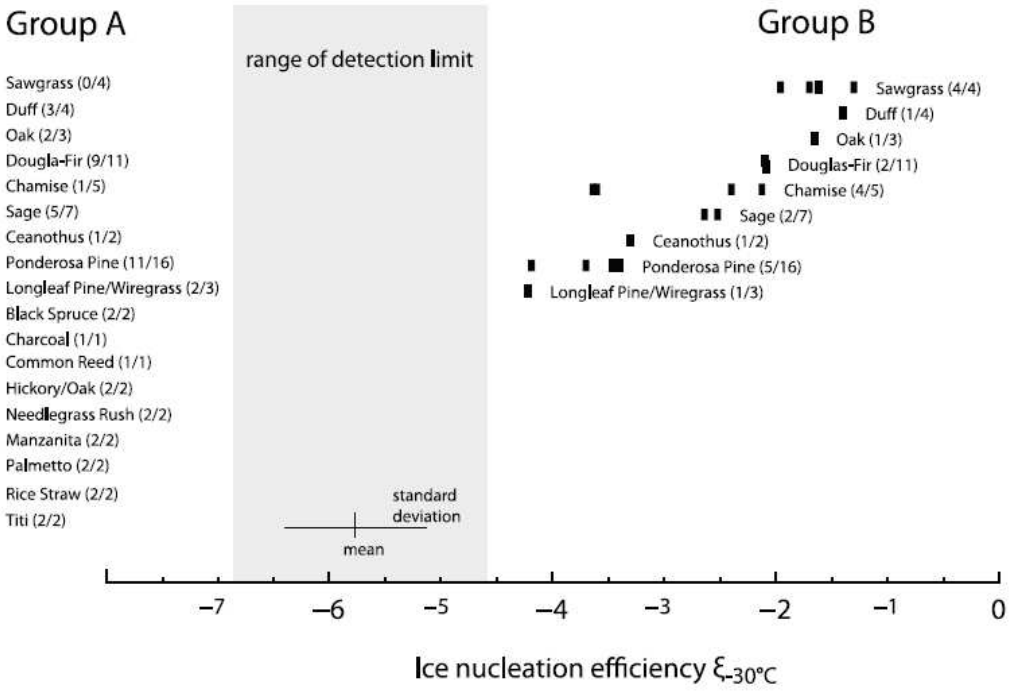

Figure 1.5. Fuel type as a function of ice nucleation efficiency at -30 °C. From Petters et al., 2009, Figure 4.

Prenni et al. (2012) made ground-based field measurements at -30 °C of emissions from western U.S. wildfires and prescribed burns and found positive correlation of INPs and total particle concentrations during increased flaming (more complete) combustion and no correlation during smoldering (incomplete) combustion (more organic carbon). They also sampled a prescribed burn during the aircraft-based ICE-L study, which showed a clear spike in INP concentration during plume sampling, again indicating biomass burning as an INP source at least locally. Field measurements of INPs from wildfires were later made by McCluskey et al. (2014) between -32 and -12 °C, via sampling of two Colorado wildfire smoke plumes at a fixed surface site. These results were compared to prescribed burns in two locations and to laboratory fuel data from the FLAME 4 study. They found that wildfire plumes at a distance of up to 20 km from the source had INP concentrations of about an order of magnitude higher

than the prescribed burns sampled at less than 1 km distance and showed the potential influence of lofted mineral dust on INP concentrations in more intense fire situations. The composition of INPs from the wildfires varied, with one fire showing a majority of tarballs (suggestive of a secondary source of particulate matter, rather than a primary emission) while the other had a larger mineral/oxide particle population. There was an increase in INP concentrations during the wildfire smoke-impacted periods compared with background, but the overall fraction of INPs in particles larger than 500 nm was much lower during smoke periods, reflecting an overall lower ice nucleation efficiency than for INPs present in the background atmosphere. This is illustrated in Figure 1.6, where the red periods indicate smoke-impacted times and the INPs represent lower fractions of the total particle number concentration larger than 500 nm for both the wildfires and prescribed burns. Levin et al. (2016) also demonstrated a connection between INP emissions and Modified Combustion Efficiency (MCE) of the fire. MCE is calculated by using the excess mixing ratios of carbon monoxide (CO) and carbon dioxide (CO_2) (Ward and Radke, 1993):

$$\mathrm{MCE} = \frac{\Delta \mathrm{CO}_2}{\Delta \mathrm{CO}_2 + \Delta \mathrm{CO}} \qquad (\mathrm{Eq.}\ 1.1)$$

A higher value indicates flaming combustion and is generally associated with larger emissions of black carbon, while a lower value signifies smoldering combustion and primarily organic carbon in the aerosol emissions. The relationship found with MCE indicates a potential role of refractory black carbon serving as INPs. When refractory black carbon was removed, a reduction of INPs up to 70% was observed for select fuels. However, the potential for black carbon to serve as INPs was most commonly found for certain grass types indigenous to coastal

regions, and not for Western U.S. pine species. Consistent with McCluskey et al. (2014), the samples had low fractions of INPs.

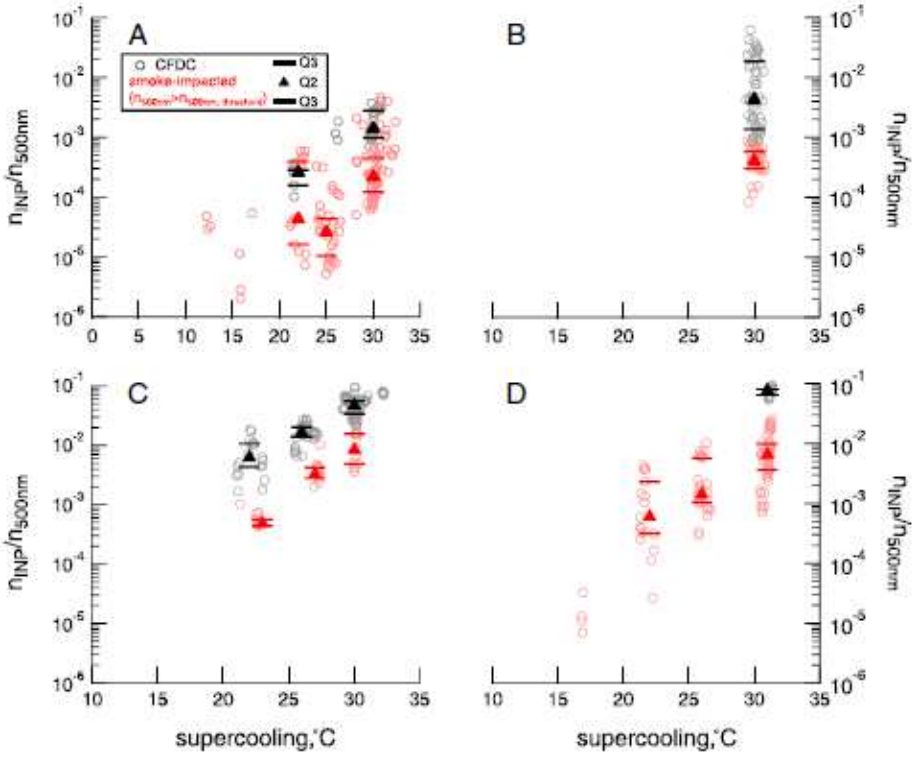

Figure 1.6. Ratio of INP concentrations to aerosol over 500 nm for prescribed burns (A and B) and wildfires (C and D) sampled). Red indicates smoke-impacted times. From McCluskey et al., 2014, Figure 5.

1.5. WE-CAN Study Overview and Study Goals

The majority of the reported INP measurements from biomass burning emissions were made at the ground level or during laboratory burns. It is clear that INPs in smoke can have at least a local influence on the atmospheric INP budget, but variability in INP emission rates vary from prescribed burns to wildfires, among various fuel types, and with the degree to which the combustion conditions are flaming or smoldering. INP measurements were made as part of the Western Wildfire Experiment for Cloud Chemistry, Aerosol Absorption, and Nitrogen (WE-CAN)

campaign in summer 2018 and are among the first free tropospheric INP measurements in smoke plumes. This study aims to use this unique dataset to:

- characterize the composition and possible sources of biomass burning INPs in emissions from several Western U.S. wildfires,
- examine how INP concentrations change with dilution, plume age, and among fires, and
- use resulting observations to understand if INPs from biomass burning can play an atmospherically relevant role above out-of-plume background air at the free tropospheric level, thereby affecting clouds and climate.

An overview of the WE-CAN payload and the specific measurements and analysis methods used in this work is provided in Chapter 2.

2. Experimental Methods

2.1. WE-CAN Overview

The Western Wildfire Experiment for Cloud Chemistry, Aerosol Absorption and Nitrogen (WE-CAN) campaign was based in Boise, Idaho during July and August 2018. Over the course of six weeks, 16 research flights (RF) were conducted on the NSF/NCAR C-130 to sample smoke-impacted clouds, aged smoke, and fresh plumes, resampling the latter as they moved downwind to study the effects of aging (an example of a plume is shown in Figure 2.1). Figure 2.2 shows the tracks of all flights, which took place over Washington, Oregon, Idaho, Montana, Nevada, and California. Most measurements were made in the free troposphere, with a notable exception in RF8 that took place in the Central Valley boundary layer. There was a full payload on board to sample gas-phase and aerosol chemistry as well as cloud water and cloud droplet residuals (Figure 2.3). Measurements included: nitrogen oxides (NO_x), ammonia (NH_3), nitrous acid (HONO), aerosol concentrations and composition, black carbon, many volatile organic compounds (VOCs) and smoke tracers, including carbon monoxide (CO). Two primary inlets, with different aerosol passing characteristics, supplied samples to the onboard instrumentation, whereas additional instruments sampled from wing pods as indicated.

The plume sampling strategy of WE-CAN was pseudo-Lagrangian, measuring most plumes between 30 minutes and 5 hours of aging, and resampling according to the prevailing wind speed carrying the plume (Figure 2.4). This sampling approach resulted in the plane initially sampling behind the fire for a background measurement and then making plume transects away from the fire perpendicular to the wind direction. Flight restrictions and communication with air traffic control determined the spatial zone that the plane could travel.

Figure 2.1. The NSF/NCAR C130 transiting near the Goldstone Fire in Montana as part of research flight 11. Photo by Kevin Barry.

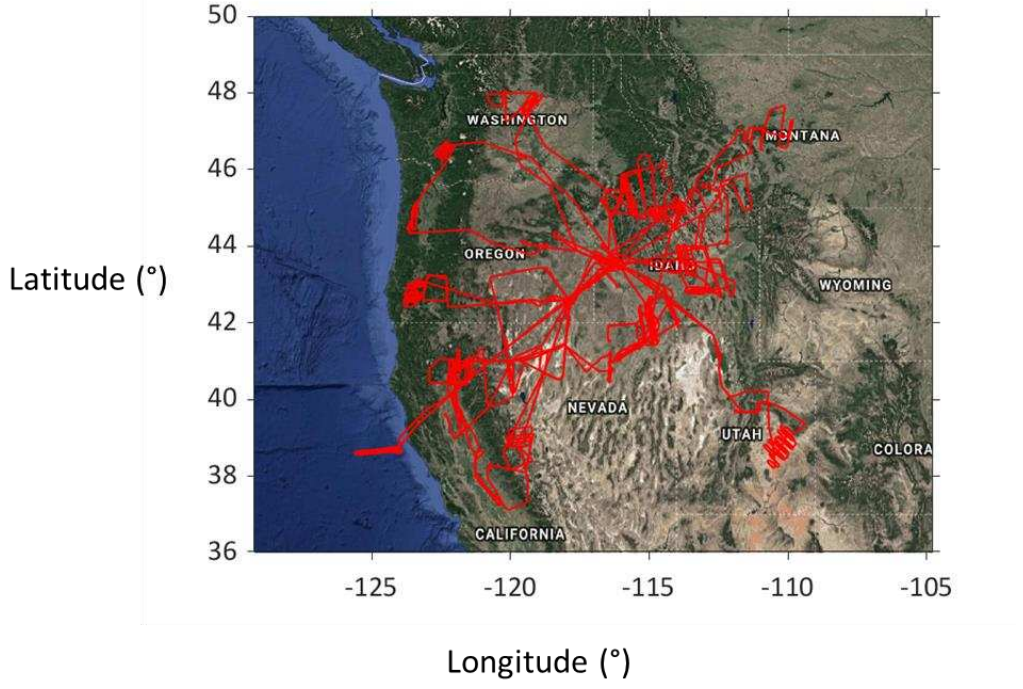

Figure 2.2. Flight tracks of the NSF/NCAR C-130 in red for all 16 research flights from July-August 2018.

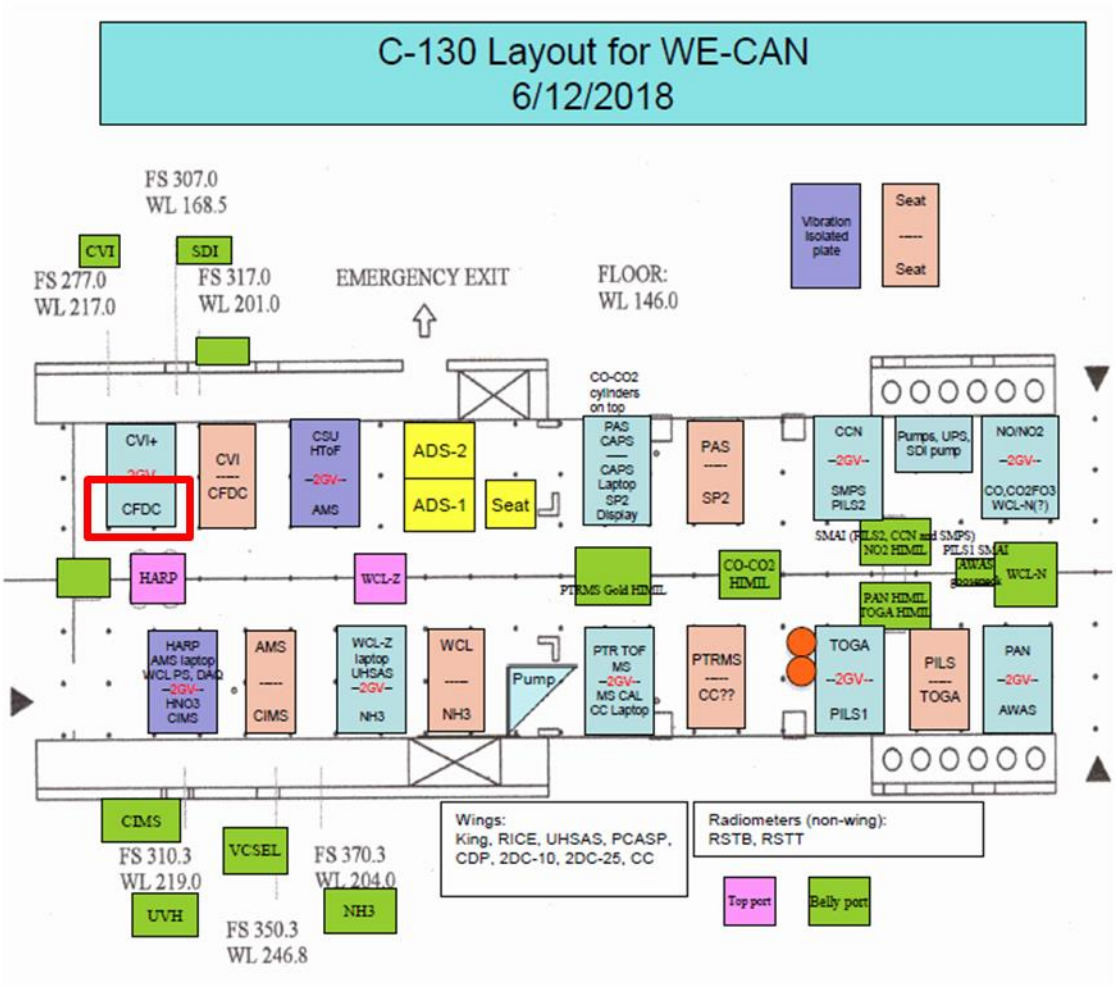

Figure 2.3. Location of the instruments onboard the NSF/NCAR C-130 for the WE-CAN campaign. The position of the CFDC and filter collections are highlighted in the red box. Sampling was from the SDI (CFDC and filters) and CVI (CFDC) inlets.

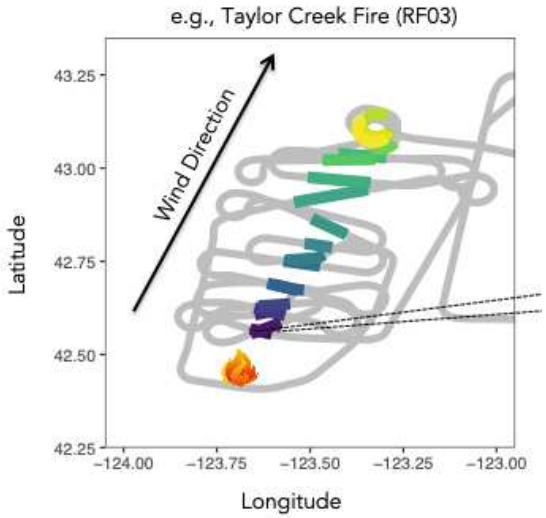

Figure 2.4. Plume sampling strategy example for WE-CAN that initially sampled upwind of the fire for background, then moved downwind in a pseudo-lagrangian method for plume aging. Credit: Jakob Lindaas.

2.2 Instrumentation Used in Analysis

The main instruments that collected data used in this thesis are shown in Table 2.1. The Continuous Flow Diffusion Chamber (CFDC) is an online ice nucleation instrument that measured on the aircraft, whereas aerosol filters were collected onboard to be analyzed later at CSU with the Ice Spectrometer (IS). Both the filters and the CFDC were positioned on the front starboard side of the C-130 (highlighted in Figure 2.3) and connected to the Solid Diffuser Inlet (SDI) to transport ambient aerosol particles into the cabin. The CFDC also sampled off a Counterflow Virtual Impactor (CVI) inlet to measure cloud droplet residuals in real time, but those data are not presented here. Pictures of the aircraft setup for the CFDC and filter collections are shown in Figures 2.5 and 2.6.

Table 2.1. Table of the instruments and their corresponding measurement used in this analysis.

Instrument	Measurement	Inlet
Continuous Flow Diffusion Chamber (CFDC)	Ice Nucleating Particles (INPs)	SDI/CVI
Aerosol filter collections for the Ice Spectrometer (IS)	Ice Nucleating Particles (INPs)	SDI
Ultra-High-Sensitivity Aerosol Spectrometer (UHSAS)	Aerosols from 0.06 µm to 1 µm	Wing-mounted
Passive Cavity Aerosol Spectrometer Probe (PCASP)	Aerosols from 0.1 µm to 3 µm	Wing-mounted
Trace Organic Gas Analyzer (TOGA)	Volatile organic compounds mixing ratios	HIMIL
Aerodyne CS-108 miniQCL	CO, N_2O, H_2O mixing ratios	HIMIL

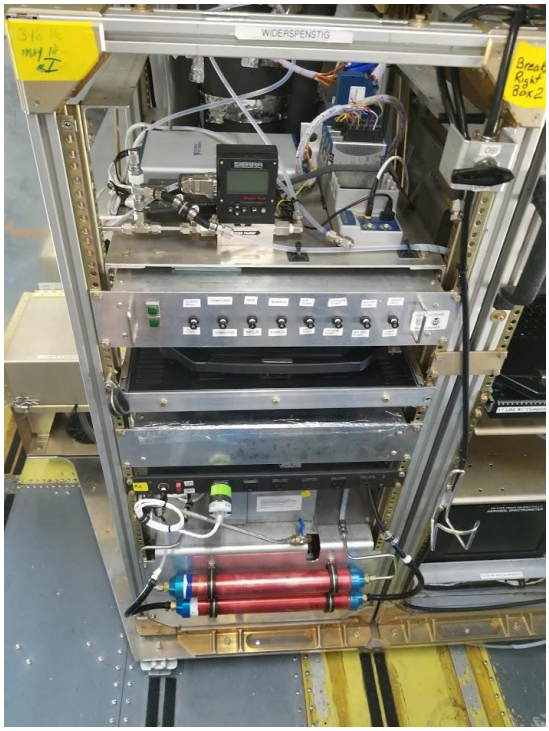

Figure 2.5. The CFDC onboard the NSF/NCAR C-130.

Figure 2.6. The filter collection setup on the NSF/NCAR C-130 for analysis with the IS. Two filters were loaded at any given time, for switching when inside and outside of plumes. Total flow rates were monitored in real-time with the flow meter visible in the upper right.

2.2.1. Gas Phase Measurements

Biomass burning is a large source of carbon monoxide (CO) from incomplete combustion. The tropospheric mixing ratio is generally between 40 and 200 ppbv (Seinfeld and Pandis, 2016). In WE-CAN, CO was measured from the Aerodyne CS-108 miniQCL at 1 Hz data and was used extensively as a smoke tracer and helped determine the plume times (Section 2.4.1). The uncertainty at 95 percent confidence is estimated +/- 1 ppbv. An example of a CO timeseries from the South Sugarloaf (RF15) fire is illustrated in Figure 2.7.

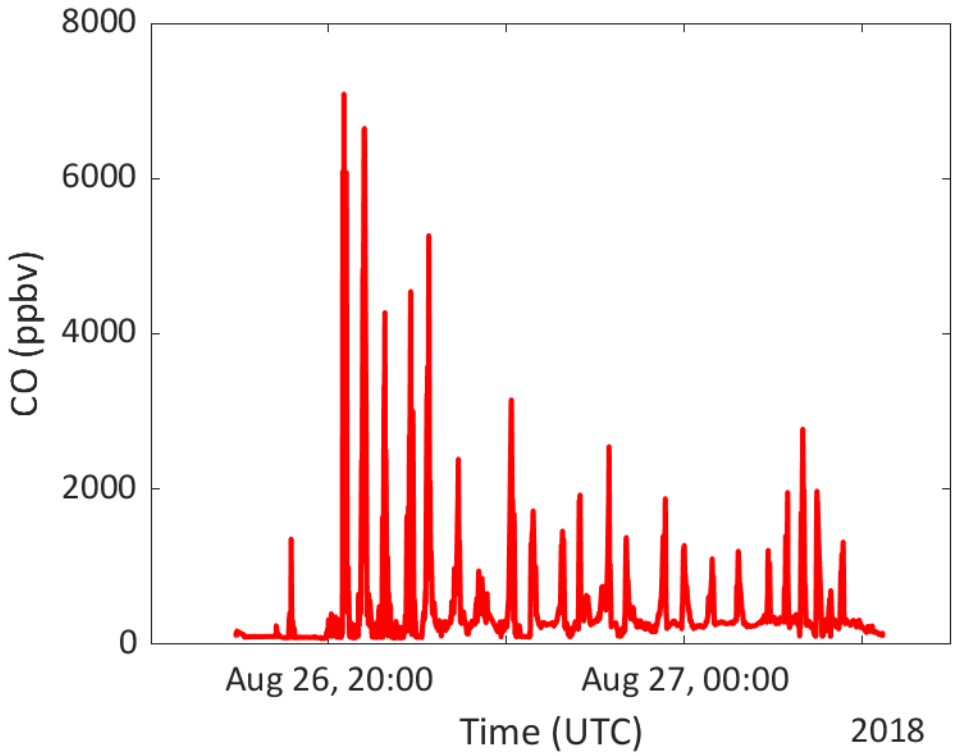

Figure 2.7. CO timeseries for the South Sugarloaf (RF15) fire on August 26, 2018. Plume passes are indicated where CO concentrations are highly elevated above surrounding regions.

WE-CAN sampled a unique set of airmasses with emissions from the burning of several fuel types, not only fresh plumes, but also extensive regions of mixed-age smoke from multiple sources. Since parts of the western United States (California in particular) have urban and pollution influence, those emissions likely mixed with some of the smoke sampled by the aircraft, depending on location. A large collection of VOCs were measured, and some of those compounds can be used as tracers to determine which sampling time periods were more affected by mixing with pollution. Light alkanes are predominantly found in regions with oil and natural gas production but also come from vehicle emissions and biomass burning. The ratio of isopentane to n-pentane is useful to help separate airmasses, as tailpipe emissions contain elevated levels of isopentane over n-pentane, leading to higher ratios in urban areas compared

with air masses that are influenced only by biomass burning (Thompson et al. 2014). The potential role of pollution on INP number concentration has been looked at previously, with Bi et al. (2019) finding lower INP concentrations during pollution events in China than dust-impacted periods, but higher than clean periods. They found pollution events may increase INPs, but much less than the increase of total particle concentrations. In a laboratory study, Schill et al. (2016) measured INP concentrations from diesel exhaust at 0 and 1.5 days of photochemical aging but did not find measurable INP concentrations in spite of elevated total particle and black carbon concentrations.

Both isopentane and n-pentane were measured with the Trace Organic Gas Analyzer (TOGA) instrument that was onboard the NSF/NCAR C-130 and this data was used to separate urban influence from biomass burning for INP concentrations. The most notable flight for urban influence in WE-CAN was RF8 during the sampling of the boundary layer of the Central Valley in California. The extent of urban influence in other plumes were also estimated using the iso- to n-pentane ratios.

2.2.2. Aerosol Counting and Sizing Instrumentation

Two aerosol sizing instruments were used in this work, the Passive Cavity Aerosol Spectrometer Probe (PCASP) and the Ultra-High Sensitivity Aerosol Spectrometer (UHSAS). Both instruments were wing-mounted during WE-CAN. Sizing is done based on the intensity of scattered light from a laser. The size range of these instruments is given in Table 2.1. There is some uncertainty in the use of these instruments for particle concentration and surface area, such as from the assumption of spherical particles. However, uncertainty is quantified in Kupc et al. (2018) for free tropospheric sampling for 1 minute integration times as approximately 6

percent for number concentration and approximately 36 percent for surface area measurements for the UHSAS (which is taken here as an estimate for the PCASP as well). The data from these instruments are used for normalizations and instrument time stamp alignment, which will be described further in this chapter.

2.3 Ice Spectrometer

The CSU Ice Spectrometer (IS) is a laboratory-based instrument designed to analyze filter suspensions for INPs in the immersion freezing mode. The present version is based on developments from Hill et al. (2014; 2016) and recently described in DeMott et al. (2018). Aerosol filter samples were collected on the C-130 with two 47-mm diameter in-line aluminum filter holders with 0.2 μm pore diameter Nuclepore polycarbonate filter membranes. Additionally, filters of 10 μm pore diameter were used for backing these filters in the sample holders (to prevent any potential contamination from the metal mesh screen in the inline filter holders). The filters were precleaned with 10 percent hydrogen peroxide (H_2O_2) and two deionized (DI) water rinses. The filter holders were cleaned after each flight with 5 percent H_2O_2 and DI water rinses. The two holders allowed for efficient alternating between plume and out-of-plume background filters, controlled with the manual valve switching system shown in Figure 2.6 . The timing for switching exposure of the plume and background filters was determined using real-time CO mixing ratios from the Aerodyne CS-108 miniQCL onboard the aircraft as well as from flight tracks and information relayed from the cockpit. Mass flow rates were recorded at 1 Hz intervals to tabulate total volume filtered. Filter samples were placed into sterile 50 mL Falcon polypropylene centrifuge tubes and stored frozen for transport back to CSU.

The filters were taken out of the freezer immediately before individual analysis and 7 mL of 0.1 µm-filtered DI water were added to each tube. The tubes were placed in a Roto-Torque Rotator set at 1 cycle s^{-1} for 20 minutes to release particles into liquid, creating a suspension. 50 µL aliquots of the samples were then dispensed into 96-well PCR plates in blocks of 32, typically using 1.6 mL of the original suspension. Remaining suspension was frozen for use in treatments, as discussed below. All preparation was done in a HEPA-filtered, laminar flow hood to ensure cleanliness. Next, the PCR plates were placed into two aluminum blocks in the IS, which cools at approximately 0.33 °C min^{-1}. A camera automatically detects when wells freeze and records data at one-second intervals, however, images are only saved every 60 seconds (Figure 2.8). A 0.1 µm DI water blank of 32 wells was also dispensed with every run for post-processing corrections and used to set the lower temperature limit for the test. This was typically between -27 and -29 °C, when the difference in the number of frozen wells in the sample versus the blank is no longer distinguishable.

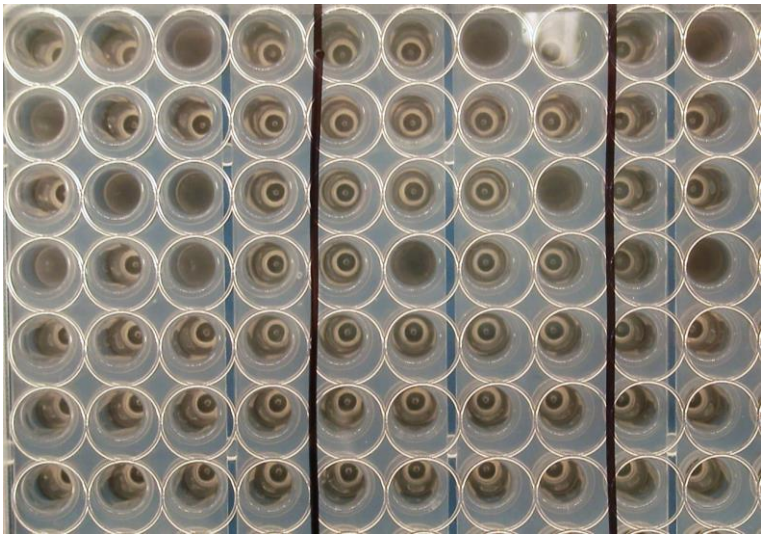

Figure 2.8. An example of wells freezing (darker color) that are camera-detected and recorded for analysis. Credit: Thomas Hill.

Cumulative INP concentrations were determined by first calculating the INPs per mL of sample liquid based on Vali (1971):

$$N_{INP(mL^{-1})}(T) = -\frac{\ln\left(f_{unfrozen}(T)\right)}{V_{drop}} \quad \text{(Eq. 2.1)}$$

where $f_{unfrozen}$ is the fraction of droplets not frozen at temperature T and the V_{drop} is the volume of the individual droplets (in this case 50 µL). Equation 2.1 accounts for the probability of droplets that freeze at warmer temperatures containing INPs that would initiate freezing at colder temperatures. Next, the concentration of INPs per mL was converted to the concentration per L of air:

$$N_{INP(L^{-1})}(T) = \frac{N_{INP(mL^{-1})}(T) * d * V_s}{V_{air}} \quad \text{(Eq. 2.2)}$$

where d is the level of dilution (1 if no dilution), V_s is the volume of the suspension in mL, and V_{air} is the total volume of air filtered in standard liter output from the mass flow meter. Since these filters were primarily collected in the free troposphere, few dilutions were needed, but the most commonly used dilution was 15-fold (200 µL sample and 2800 µL 0.1 µm-filtered DI water). The volumes of air filtered were generally around 100-500 liters but were dependent on the altitude (less flow rate with increased altitude) and the time spent sampling a particular plume. Generally, only one filter was collected per plume to collect enough particles for reasonable limits of detection in the IS. A larger volume of air collected lowers the limit of detection (LOD) of the instrument, which also considers the number of wells dispensed and volumes of the droplets and suspension used:

$$\mathrm{LOD} = \frac{\left(\frac{-\ln\left(\frac{N_{wells}-1}{N_{wells}}\right)}{V_{drop}} * V_s \right)}{V_{air}} \quad \text{(Eq. 2.3)}$$

where N_{wells} is the total number of wells used (generally 32). These calculations generated cumulative INP-temperature spectra for plume intercomparisons and comparisons with prior literature. 95 percent confidence intervals (CI) were calculated based on Agresti and Coull (1998) for binomial sampling:

$$CI_{95}(T) = \frac{\left(f(T) + \frac{1.96^2}{2n} \pm 1.96\sqrt{\frac{f(T)\left(1-f(T)\right) + \frac{1.96^2}{4n}}{n}} \right)}{1 + \frac{1.96^2}{n}} \quad \text{(Eq. 2.4)}$$

where f is the frozen fraction of droplets at temperature T and n is the total number of droplets dispensed.

Peroxide digestion and thermal treatments were done on select remaining filter suspensions after analyzing all of the base spectra. These treatments provide some information about the composition of the INPs collected from smoke plumes. Heat treatments denature heat-labile organics such as proteins, while H_2O_2 digestion removes all organic material from a sample (McCluskey et al., 2018; Suski et al., 2018). The heat treatments were performed by placing a portion of the particle suspension volume into a 95 °C boiling water bath for 20 minutes. Next, the samples were cooled until they reached room temperature and were subsequently dispensed into PCR trays for analysis. For peroxide digestion, 1 mL of 30% H_2O_2 was added to 2 mL of sample suspension for a resulting H_2O_2 concentration of 10%. The solution was then placed into a 95 °C boiling water bath with ultraviolet (UV-B) lights for 20

minutes to generate hydroxyl radicals that oxidize organic carbon (Figure 2.9). The samples were cooled for 15 minutes, approximately 100 µL catalase from bovine liver was added to remove excess H_2O_2, and then the sample was dispensed for analysis. If there was a large difference in the untreated versus treated INP-temperature spectra, a dominant organic influence existed in the original filter collection, with the heat treatment indicative of the high-labile fraction thereof.

Figure 2.9. Samples being heated at 95 °C and irradiated with UV-B light to form hydroxyl radicals during the peroxide digestion treatment.

Seven field blanks were taken throughout the campaign to account for INPs on the filters at the start of the campaign (from manufacture and from pre-cleaning) and also through subsequent handling. These filters were prepared in the same way as for other filters, brought onto the plane and placed in the filter holders, and later into 50 mL Falcon tubes for transport

and analysis at CSU. Once all blanks were analyzed with the IS, a regression line was fit and used to subtract INPs from every filter at each processing temperature before converting the measurements to equivalent concentrations in air. A similar blank was carried out for the peroxide tests, where 1 mL of H_2O_2 was added to 2 mL of 0.1 µm filtered DI water instead of to a sample, to determine if INPs were added during the addition of the H_2O_2 and catalase. All concentrations are cumulative and thus increase with decreasing temperature. However, due to accounting for blanks, some INP-temperature spectra may decrease with temperature.

2.4. Continuous Flow Diffusion Chamber

The CSU Continuous Flow Diffusion Chamber (CFDC) instrument (Rogers, 1988; Rogers et al., 2001; DeMott et al., 2015) (Figure 2.10) consists of two concentric cylinders, an outer and inner wall, that have gradients in temperature and water vapor between them. The temperatures of the walls determine the supersaturation profile in the chamber with respect to ice and water. Sample air is dried with diffusion dryers and brought in at 1.5 volumetric liters per minute (standard flow recorded), with upstream aerosol impactors removing particles larger than approximately 2.5 µm. A particle-free sheath air flow of 8.5 volumetric liters per minutes is introduced, sandwiching the aerosol lamina. The supersaturation allows ice crystals to grow from activated INPs in the chamber with a total residence time of approximately 7 seconds. An evaporation region follows (approximately 1/3 of the column) where the temperatures of the two walls are set to be the same so there is no longer supersaturation with respect to water, evaporating the water droplets, but the persisting ice supersaturation conditions allow the ice crystals to both remain and grow for later detection with an optical particle counter (OPC). The operating temperature of the aerosol lamina was generally kept

around -25 °C or colder as the INP concentrations would be too low for detection at warmer temperatures during free tropospheric sampling. The water supersaturation was kept around 5% for analysis of INPs, emphasizing the immersion freezing mode for comparison to immersion freezing data from the IS (DeMott et al., 2015). Grids for transmission electron microscopy (TEM) were also collected downstream of the CFDC chamber to analyze the composition of plume INPs. The impactor is a single-jet impactor designed for a 50% cut-size of 4 microns, so as to capture only activated ice crystals.

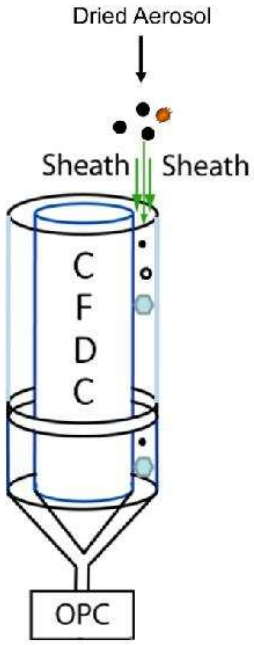

Figure 2.10. Schematic of the CFDC showing aerosol brought in, ice crystals growing in the chamber, and crystal detection with an optical particle counter (OPC). A two-stage 2.5 µm impactor is used upstream of the CFDC inlet manifold.

2.4.1. Defining Plume Versus Background Air

The time spent in plume versus background was defined by using CO mixing ratios from the Aerodyne CS-108 miniQCL. First, the CO data were filtered with a moving median to remove

noise. The moving median was chosen because it is less sensitive to outliers than a moving mean. The background periods were selected based on where the first derivative of the data outside of the main plume was small enough (not much change in time—less than 1.5 ppb/s) and the CO concentration was below an overall threshold of 300 ppb for at least one minute. The amount of smoothing had to be changed slightly throughout the campaign due to the heterogeneities of some plume backgrounds (a noisier background required more smoothing), but this method worked well overall to provide a consistent way to differentiate airmasses. Once the background periods were defined, the plume times were chosen to be the sample periods in between, with a minimum time for a plume pass defined as 30 seconds; shorter in-plume periods were not included in the analyses. Next, the plume passes were attributed to a specific fire. U.S. Forest Service collaborators provided fire center latitude and longitudes as well as times sampled for all plumes (WE-CAN field catalog). This location and time information provided bounds on the defined passes by setting latitude and longitude ranges from the fire center and making sure the passes were within the given sampling times. Background periods attributed to a single plume were selected to not extend more than three minutes before and after the overall plume start and stop times for constraint.

2.4.2. Defining Ice Versus Aerosol

The OPC of the CFDC detects both aerosol particles and ice crystals that make it through the evaporation section of the chamber. Scattered light from the diode laser in the OPC is related to the size of the particle through the amplitude of voltage pulses. Size-resolved particle counts are recorded at 1 Hz intervals. Since ice crystals are larger than unactivated particles, a bimodal distribution differentiates the two and sets a lower limit for ice crystal size. Histograms

were made for every research flight, and the first bin with 0 aerosol counts (or the minimum between the aerosol and ice distributions) was found and recorded as the maximum aerosol bin. An example for one of the flights is shown in Figure 2.11. The average of the 16 bins (one from every flight) determined the ice cutoff size: everything greater than bin 150 was classified as ice and everything below was classified as (unactivated) aerosol. Although this method has uncertainty, the histogram distributions are heavily bimodal so the exact line for the cutoff size around 150 makes little difference in the total INP counts. A recent OPC calibration indicates that this cutoff size would include ice crystals over about 3 µm.

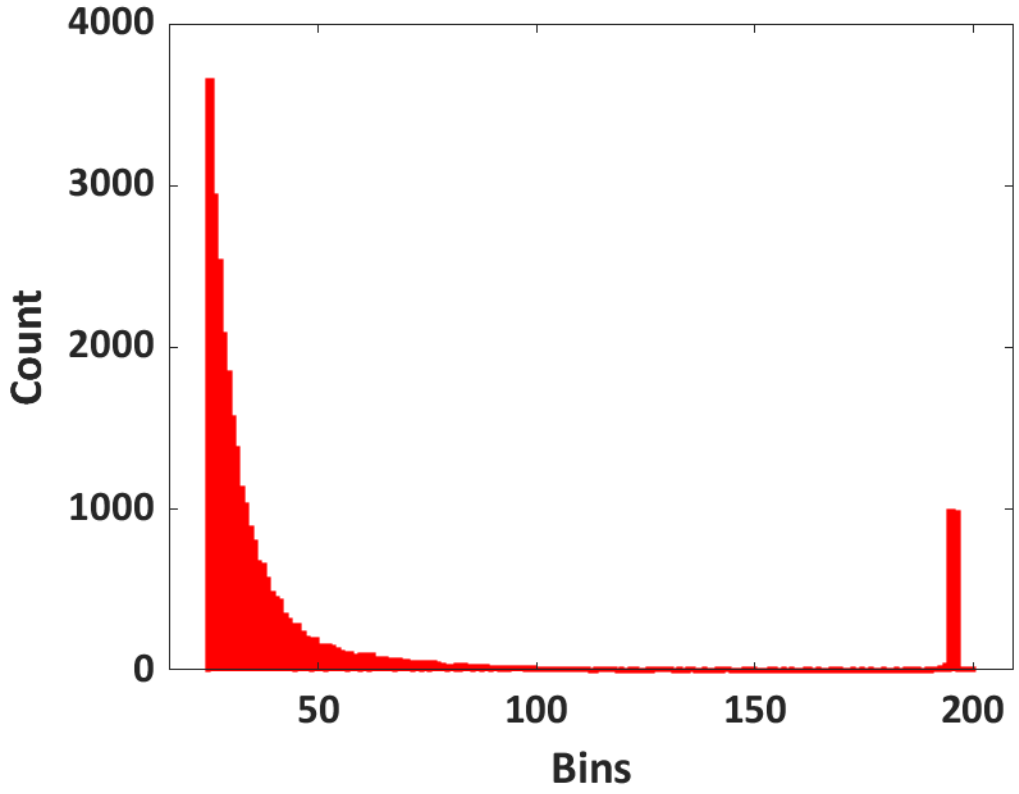

Figure 2.11. An example histogram of total counts detected by the OPC for a WE-CAN research flight.

2.4.3. Aligning Data to the PCASP

Since aircraft instruments have differing inlet configurations and time responses (due to tubing lengths, varying flow rates, and so on), all online aerosol instruments were aligned to the time stamps of the PCASP, which has the fastest time response, as it was mounted on the wing. To align the CFDC, both datasets were smoothed with a 1-2-1 filter, which is a symmetric moving average. Next, the CFDC was shifted forward in time in 1 second intervals for 100 seconds, and the correlation coefficient calculated for each shift. The second with the highest correlation coefficient determined how much to shift the CFDC data, and this process was repeated for every flight. The mean of the seconds shifted for all flights is approximately 16 seconds. An example of this process is illustrated in Figure 2.12. There are portions of flights where the peaks are not perfectly aligned, which could be due to changing time responses with altitude, but a single time shift was used for each flight, as variable alignment during an individual flight would lead to overlapping times and greater uncertainty.

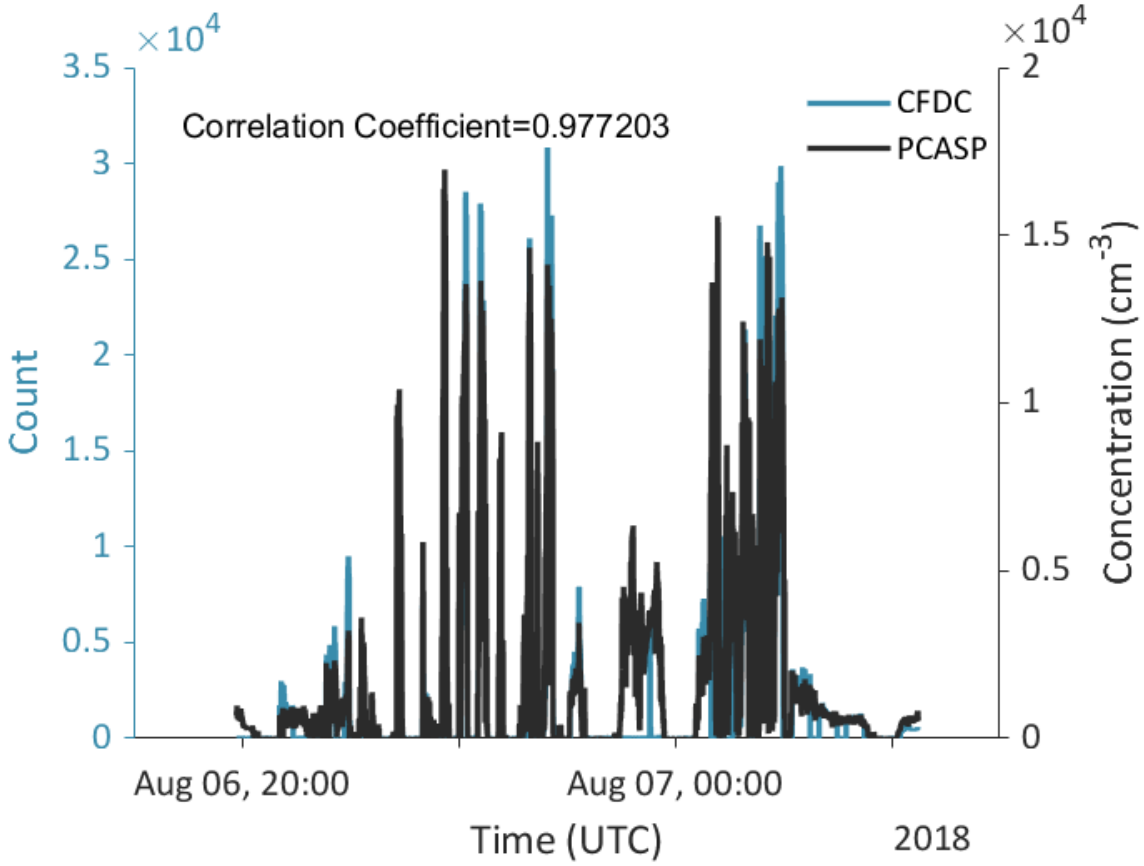

Figure 2.12. An example of peak alignment between the CFDC (total OPC counts) and PCASP (total aerosol concentration). This is corresponding to RF7, where the correlation coefficient is about 0.98 for a 19 second shift.

2.4.4. Removing Large Frost Spikes from the Data

Frost particles can occasionally break off from the CFDC walls and result in false counts at ice crystal sizes. At rare times, this occurs as a large pulse (presumably a very large amount of frost released) that can last up to several seconds. To remove this type of frost signal, histograms were made for every flight of the 1 Hz ice counts (summation of all bins above 150 for every second). Next, the minimum in the first mode of the count number distribution was found and everything above that bin was removed. This was done individually for every flight, and if any 1 Hz count exceeded the ice mode threshold, the next two seconds of data were also

removed (as frost spikes could impact the OPC for multiple seconds). For example, if a flight has a minimum mode in the count distribution of 6 ice particles per second, a spurious ice count of 20 particles per second for that flight would automatically be removed from the data. The idea is that once there is a break in continuity, everything else is likely an anomalous frost spike. This may be considered as a low-pass filter method for removing large frost counts. Persistent background counts, likely also as frost, do occur at varying degrees over time in the CFDC, and these are accounted for by filtering the sample flow and assessing the ice counts detected in the OPC size range (greater than bin 150). However, removing anomalous large frost spikes over the whole time series (during both sample and filtered air periods) is the first step before correcting sample periods for the more regular and lower levels of artifact ice crystals detected while sampling filtered air through the CFDC (discussed further in Section 2.4.5).

2.4.5 CFDC INP Concentration Calculations, Accounting for Frost Artifact Correction, and Significance Testing

Although data from the CFDC are recorded at 1 Hz, several minutes of data from the same general air mass or part of the plume were combined and averaged to determine an INP concentration point, and to improve statistical significance. As often as possible, sampling periods were 10 minutes long, bookended by five minute filter periods, but this varied based on the aircraft sampling strategies and many plume passes were often less than 10 minutes. In a filter period, sample air was drawn in through a HEPA filter to provide a filtered sample for the instrument, allowing for quantification of artifact ice crystals from low level frost emission during operation (e.g. DeMott et al. 2017). Each sample period was broken up into either a plume or out-of-plume background time (detailed above from CO data), and corresponding

filter periods on either side of a sample pass were determined to comprise one filter vector of ice counts. If there were multiple CFDC sampling periods within a plume or plume-background pass, a combined sample ice count vector was created. Data with water supersaturation larger than 10 percent or less than 2 percent for sample periods and less than 0 percent for filter periods were replaced with NaNs (not a number) to remove them from subsequent calculations. These thresholds are based on previous studies such as Petters et al. (2009) that show droplets can survive the evaporation region and be false counted at ice crystal sizes at water supersaturations larger than 10 percent. A too low water supersaturation results in inefficient activation of ice crystals in the proximal immersion freezing mode. For WE-CAN, measurements were generally made at supersaturations between 4 and 8 percent, but aircraft changes in direction and altitude that affected refrigeration system control through thermal and airflow changes around compressor heat exchangers sometimes made this challenging.

Poisson distribution rate parameters (lambdas) were then calculated as shown below for the sample and filter ice count vectors by dividing the ice count (x) by the total measuring time in seconds (n) for the period. A NaN did not impact either x or n.

$$\lambda_{\mathrm{filter}} = \frac{\mathrm{x_{filter}}}{\mathrm{n_{filter}}} \qquad \text{(Eq. 2.5)}$$

$$\lambda_{\mathrm{sample}} = \frac{\mathrm{x_{sample}}}{\mathrm{n_{sample}}} \qquad \text{(Eq. 2.6)}$$

Next, 95 percent confidence bounds and testing for significance were determined following the method in Krishnamoorthy and Lee (2012) for the moment confidence interval. This specific method is newly implemented for the CFDC data, since Schill et al. (2016), and is ideal for data periods that have smaller rate parameters. It is also a good choice if the filter

periods are different lengths of time as it uses one combined vector. It tests whether the rate parameter for a given sample period is different from the filter period. The z-values were calculated by:

$$Z = \frac{\lambda_{sample} - \lambda_{filter}}{\sqrt{\lambda_{total} * \left(\frac{1}{n_{sample}} + \frac{1}{n_{filter}}\right)}} \quad \text{(Eq. 2.7)}$$

where the total rate parameter was calculated by:

$$\lambda_{total} = \frac{x_{filter} + x_{sample}}{n_{filter} + n_{sample}} \quad \text{(Eq. 2.8)}$$

If the calculated z-value was greater than the z-value for 95 percent confidence for a one-tailed normal distribution (1.6449), as well as if the product of n and lambda was greater than or equal to 10 for the sample period and greater than or equal to 5 for the filter period, the sample period was flagged as showing a statistically significant increase in INPs versus the filtered air period (signal of aerosol sample over frost). This normal approximation improves for a larger product of n and lambda, but these were set as the minimum thresholds. Confidence intervals (CI) also follow from Krishnamoorthy and Lee (2012) and were calculated by:

$$CI = \lambda_{sample} - \lambda_{filter} + \frac{z_{0.95}^2}{2}\left(\frac{1}{n_{sample}} - \frac{1}{n_{filter}}\right) \pm z_{0.95}\sqrt{\left(\frac{\lambda_{sample}}{n_{sample}} + \frac{\lambda_{filter}}{n_{filter}}\right) + \frac{z_{0.95}^2}{4}\left(\frac{1}{\lambda_{sample}} - \frac{1}{\lambda_{filter}}\right)^2} \quad \text{(Eq. 2.9)}$$

Next, the CFDC filter-corrected cumulative INP concentrations for sample periods were calculated from the difference in lambdas and average flow rate ($\bar{v}$; Ls^{-1}) over the identical sample time periods:

$$N_{INP} = \frac{(\lambda_{sample} - \lambda_{filter})}{\bar{v}} \quad \text{(Eq. 2.10)}$$

where the sample flow rate is recorded at 1 Hz from the CFDC. The confidence interval lambdas are also converted to concentration by dividing by the average sample flow rate. The final units of the INP concentrations are in number per standard liter. Note that it is possible to have positive N_{INP} without meeting the significance test.

2.5. Methods to Normalize INP Data

Calculating ambient INP concentrations for fires during WE-CAN is important to quantify overall influence, but for comparison among fires studied during the campaign and previous measurements, normalizations are needed to account for different absolute magnitudes due to varying emissions rates, dilution levels, and locations at the time of measurement. Here, we describe three ways to normalize the INP data to understand the fire impact on INPs.

2.5.1. Number Concentrations of Particles Larger than 500 Nanometers

A prior published method for normalizing INP data is to calculate the ratio of the observed INP concentrations to the concentrations of particles with diameters larger than 500 nm (N_{500}). DeMott et al. (2010) found a relationship between INP concentrations and N_{500} as a function of temperature from analyzing data from nine field studies over several years. The proposed relationship between INPs and the large-particle fraction of the total aerosol is based on the expected roles as INPs of mineral and soil dust particles, as well as some biological aerosols. This normalization has been used in McCluskey et al. (2014) on the ground-based smoke-influenced INP measurements for the High Park wildfire and Georgia prescribed burns, which makes this an invaluable exercise for comparison. McCluskey et al. (2014) found N_{500} values between approximately 1 and 100 cm^{-3} for the Hewlett and High Park wildfires and up to 1000 cm^{-3} for the Georgia prescribed burns. In this work, in-plume CFDC INP concentrations

were divided by N_{500} from the wing-mounted UHSAS averaged over the same times as the defined plume passes. In doing so, dry plumes are assumed, such that relative humidity did not exceed values that would influence the ratio via hygroscopic growth.

2.5.2. Surface Active Site Density Parameter

Another INP normalization method that has been used previously is the surface active site density parameter (n_s) (Niemand et al., 2012; DeMott et al., 1995), which divides the INP number concentrations by the total aerosol surface area presumed to represent a certain INP source. Previously, n_s has been used to describe the number of ice nucleating sites carried by specific types of aerosols such as desert dust and soot measured in the laboratory (Ullrich et al., 2017), and for particles in clean marine air (McCluskey et al., 2018). This approach assumes that nucleation is a surface phenomenon, and that variability in INP concentrations are due solely to aerosol size distributions and mass loadings, and hence can be captured by normalizing for aerosol surface area. For the WE-CAN data, surface area measurements were derived from the PCASP instrument (capturing the size distribution for diameters below 2.5 μm) averaged over the CFDC sample period. This parameter has a major dependence on aerosol type, as Ullrich et al. (2017) found an n_s of approximately 6.3×10^{10} m^{-2} for dust at -30 °C, while McCluskey et al. (2018) only found an n_s of approximately 3.5×10^{7} m^{-2} for clean marine air at the same temperature. These results show that dust is a much more efficient ice nucleation source particle type than the sea spray aerosols that are sources of INPs in a clean marine environment, but the overall effect of aerosol type on INP concentrations depends on the total amount present.

2.5.3. Normalized Excess Mixing Ratio

A third normalization method that has been used extensively to describe emission rates in biomass burning for chemical species – but heretofore has not been applied to INPs – is the Normalized Excess Mixing Ratio (NEMR). NEMR is a way to understand how a species is changing with dilution in a plume, where the species of interest is x and the elevation over background is Δx. To account for dilution, a relatively constant fire tracer is chosen for normalization, which for this analysis is carbon monoxide (CO). NEMRs have been primarily calculated for chemical species like ozone, volatile organic compounds, and aerosol mass concentrations (Garofalo et al., 2019), but here we apply this concept to INP number concentrations, with units of $L^{-1}ppb^{-1}$.

$$\mathrm{NEMR} = \frac{\Delta \mathrm{N_{INP}}}{\Delta \mathrm{CO}} = \frac{\mathrm{N_{INP\ plume}} - \mathrm{N_{INP\ background}}}{\mathrm{CO_{plume}} - \mathrm{CO_{background}}} \qquad (\mathrm{Eq.}\ 2.11)$$

If there are no chemical or physical processes occurring other than dilution, the NEMR should remain constant in time as the plume ages. If the NEMR does change, it implies a source or sink of INP with aging. However, there are uncertainties associated with these calculations, as Yokelson et al. (2013) points out, if sampling occurs in conditions for which the background airmass is dissimilar to the fire source. Values of NEMR are also sensitive to the conditions chosen as background.

For NEMR calculations, out-of-plume background values had to be determined for each of the sampling periods. For carbon monoxide, background concentrations were chosen to be the average of 15 seconds of observations before and after the defined plume pass time to be consistent with the inter-transect method calculated in Garofalo et al. (2019). For INP concentration backgrounds, one number combining all background periods for each fire was

determined for subtraction from individual plume passes for better characterization of the airmass (from having a longer integration time) and to account for if plume passes did not have an adjacent background pass. This was necessary because background periods generally had lower INP concentrations that were sometimes negative after correcting for CFDC filter periods and using only 15 seconds before and after the plume is not possible. One example for not having an adjacent background pass is if the CFDC was sampling filtered air upon entering the plume or if the supersaturation was too high or low. For some flights, CO data revealed the plume-background airmass to be asymmetrical from the plume being emitted into an atmosphere with other fresh plumes or earlier plume remnants (Table 2.2, 2.3). The Taylor Creek (RF3) fire background was generally very clean and CO was nearly the same on either side of the fire, where the South Sugarloaf (RF15) fire had a dirtier and much more variable background. This could potentially affect the NEMR calculations based on the definition of background, but Garofalo et al. (2019) noted good agreement between using the inter-transect method of the average of 15 seconds on each side and a single fire-averaged background for the total organic aerosol NEMR.

Table 2.2. Table of the background values of CO in ppb for the Taylor Creek (RF3) fire.

Pass	CO before (ppb)	CO after (ppb)
1	68	73
2	70	74
3	67	78
4	68	79
5	70	73
6	71	76

Table 2.3. Table of the background values of CO in ppb for the South Sugarloaf (RF15) fire.

Pass	CO before (ppb)	CO after (ppb)
1	256	122
2	169	92
3	90	86
4	110	98
5	91	279
6	281	286
7	263	389
8	190	234
9	258	211
10	244	287
11	310	268
12	333	343
13	332	325
14	297	291
15	226	311

To find the plume age, the distance was calculated between the fire center as determined by the U.S. Forest Service collaborators (WE-CAN field catalog) and the individual plume pass. The distance was then divided by the average wind speed during the plume pass as measured by the NSF/NCAR C-130 to get plume age.

3. Results and Discussion

3.1. Overview of Analyzed Airmasses

Data from six fires during the WE-CAN campaign were analyzed for INP characteristics. The selected flights are shown in Table 3.1 and represent those for which there were multiple passes through each fire plume, and the CFDC was at good operating conditions for measurements (enough signal over filtered-air periods to pass the significance test). Each of these flights also had an aerosol filter collection with sufficient air volume to permit analysis via the IS, so that the resulting INP spectra could be compared with CFDC point measurements. The fuels burned in these fires are presented in Table 3.2. Each fire had a different main fuel type, although several fuels comprise each fire, with only the two leading ones shown here. The locations of the intensive sampling and the flight tracks are shown in Figure 3.1.

Additionally, we present data from two other flights that sampled aged smoke (RF5 and RF8) from an amalgamation of fires (Table 3.3 and Figure 3.2). These cases serve as a point of comparison to the data for single plumes.

Table 3.1. Summary of the fires and corresponding flights sampled by the CFDC that are further analyzed. The altitude range of the aircraft when the CFDC was sampling is given as meters above sea level.

Flight	Date	Fire Name	Location	Altitude Range CFDC (m)
RF03	7/30/2018	Taylor Creek Fire	Oregon	3342-3715
RF07	8/6/2018	Donnell Fire	California	4215-4556
RF09	8/9/2018	Bear Trap Fire	Utah	4527-4559
RF11	8/15/2018	Shellrock Fire	Montana	3156-3164
RF13	8/20/2018	Mendocino Complex Fire	California	4317-4625
RF15	8/26/2018	South Sugarloaf Fire	Nevada	3658-4608

Table 3.2. Fuel type summary for the 6 wildfires studied. The two most abundant fuels are given, with percentages calculated from acreage data.

Flight	Predominant Fuel Types
RF03	Douglas-fir-madrone-tanoak forest **(54%)**
	Jeffrey pine-ponderosa pine-Douglas-fir-California black oak forest **(17%)**
RF07	Red fir forest **(40%)**
	Douglas-fir-sugar pine-tanoak forest **(32%)**
RF09	Pinyon-Utah juniper forest **(32 %)**
	Interior Douglas-fir-ponderosa pine/gambel oak forest **(13%)**
RF11	Subalpine fir-lodgepole pine-whitebark pine-Engelmann spruce forest **(40%)**
	Limber pine-ponderosa pine forest **(15%)**
RF13	Chamise chaparral shrubland **(25%)**
	Jeffrey pine-ponderosa pine-Douglas-fir-California black oak forest **(16%)**
RF15	Sagebrush shrubland **(41%)**
	Quaking aspen forest **(34%)**

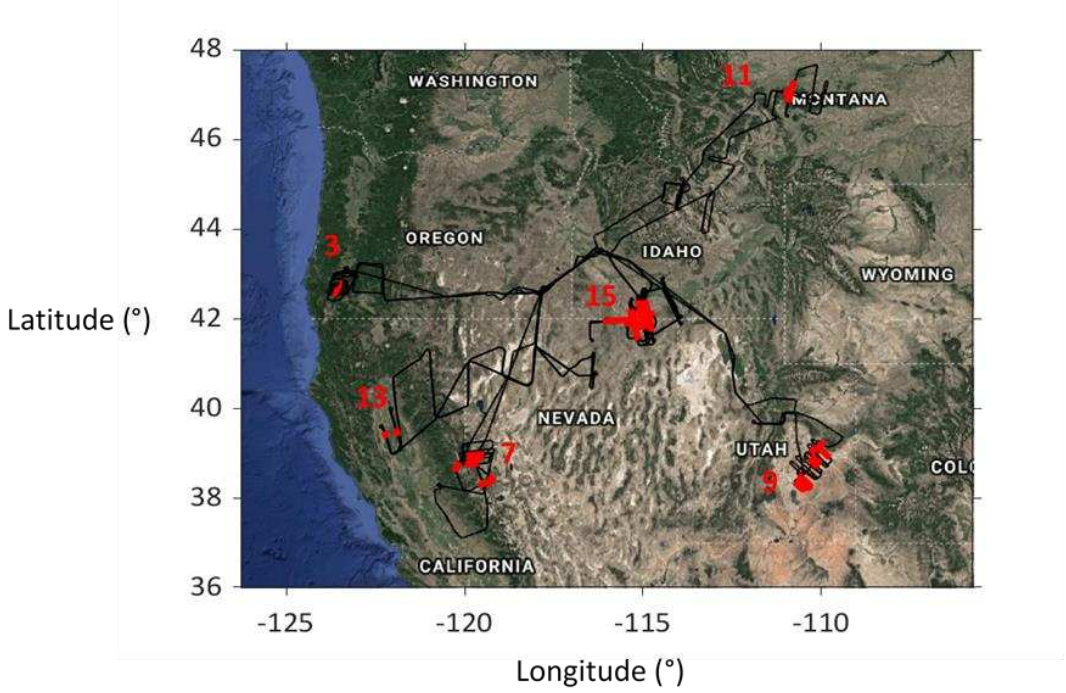

Figure 3.1. Flight track of the NSF/NCAR C-130 in black with CFDC sampling areas in red for the six wildfire plumes analyzed.

Table 3.3. Summary of the aged smoke airmasses sampled by the CFDC that are investigated further in this work. The altitude range of the aircraft when the CFDC was sampling is given as meters above sea level.

Flight	Date	Description	Location	Altitude Range CFDC (m)
RF05	7/30/2018	River of smoke	California, Oregon, Idaho	3657-4575
RF08	8/8/2018	Central Valley boundary layer	California	1574-4324

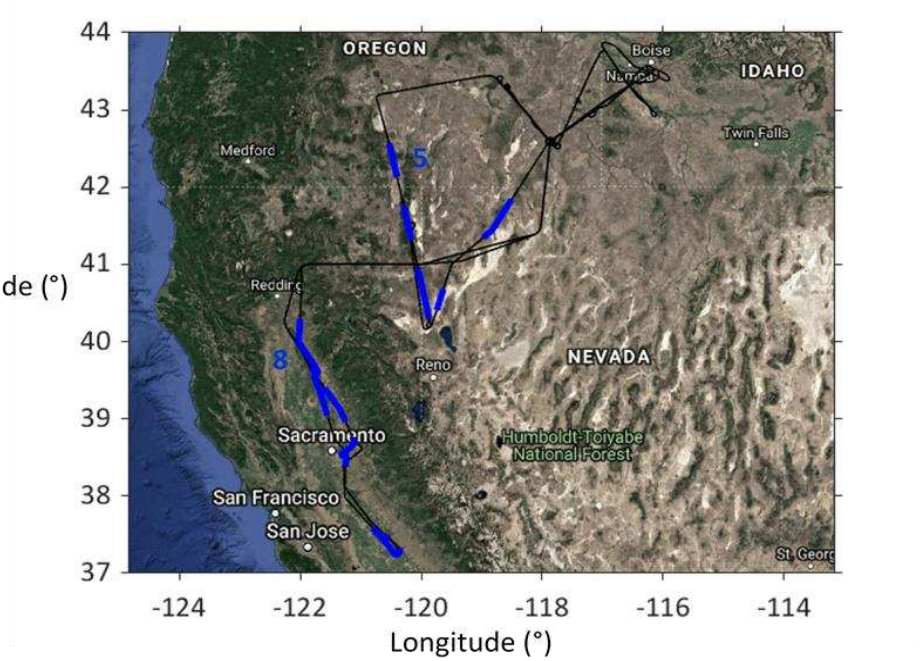

Figure 3.2. Flight track of the NSF/NCAR C-130 in black with CFDC sampling areas in blue for the two aged smoke flights.

3.2. INP Measurement Results

An overview plot of INP number concentrations (corrected to standard conditions here, and throughout this thesis) as functions of temperature are shown in Figure 3.3. This figure presents data from both the CFDC and IS for the eight cases studied (six wildfires and two aged smoke flights). All INP-temperature spectra show cumulative concentrations and are plotted on a logarithmic scale due to concentrations spanning several orders of magnitude. Only CFDC data passing the level of significance (as described in 2.4.5) are plotted. Each CFDC point represents approximately 5-10 minutes of sampling while each IS filter represents about 15-60

minutes of sampling, though there are variations based on the time spent in each plume and pass lengths. There is generally good agreement between the two methods with several regions of overlap, although the CFDC data for some passes in a number of flights are about an order of magnitude higher in concentration; possible reasons for these differences will be explored in Section 3.4. The INP concentrations for all cases are within approximately two orders of magnitude of each other at a given temperature and there are no obvious systematic differences between the spectra for the aged smoke samples compared with those from the other flights. The concentrations measured in WE-CAN are within the expected range of many previous field studies (including some biomass burning data) in Figure 1.4 (from Kanji et al., 2017) that showed INP concentrations generally between 1 and 10 L^{-1} at -25 °C. In order to further compare with previous measurements and between fires in WE-CAN, results from the normalization methods are presented next.

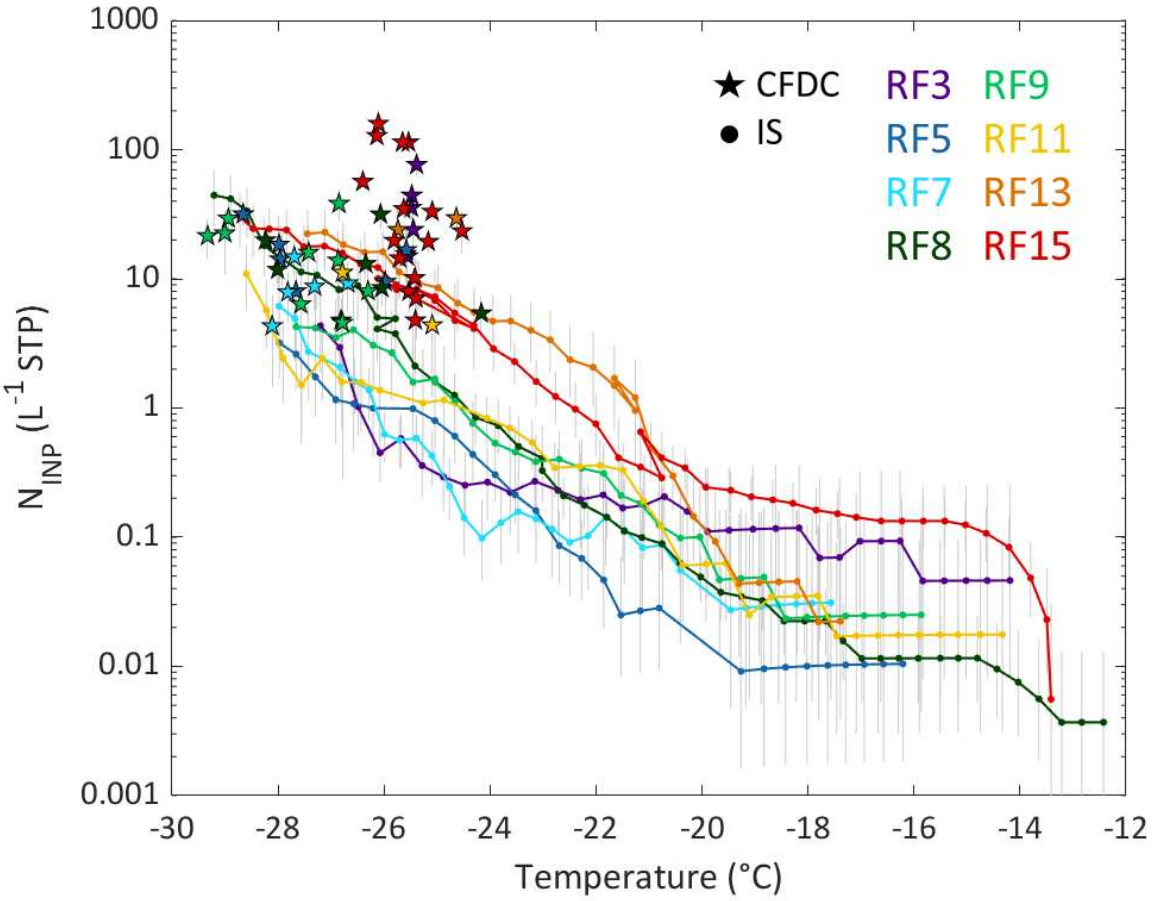

Figure 3.3. INP number concentration versus temperature, colored by research flight. The stars are data from the CFDC while the circles are data from the IS. The 95 percent confidence intervals are given in gray.

3.2.1. Scaling of INP Concentration to the Number Concentration of Particles Larger than 500 Nanometers

The results from the N_{500} normalization, which allows for comparison to plume data from McCluskey et al. (2014), are shown in Figure 3.4. The WE-CAN data are generally consistent with prior measurements, with significant overlap with the High Park wildfire. The Georgia prescribed burn values are generally lower than the data from the High Park wildfire and WE-CAN, but there is a lot of variability. The highest ratios of N_{INP} to N_{500} come from RF5

sampling the River of Smoke (some periods even higher than the High Park fire for equivalent processing temperatures), while the lowest come from RF7 sampling the Donnell fire that had a predominant red fir fuel type. There is a general trend of an increasing ratio with decreasing temperature, and the WE-CAN data collected in the free troposphere are thus consistent with the smoke plume data collected at the surface in prior efforts for wildfire measurements. It is not surprising that the prescribed burn data do not overlap with WE-CAN as they generally have lower intensities and plumes that cover smaller areas (Williamson et al., 2013).

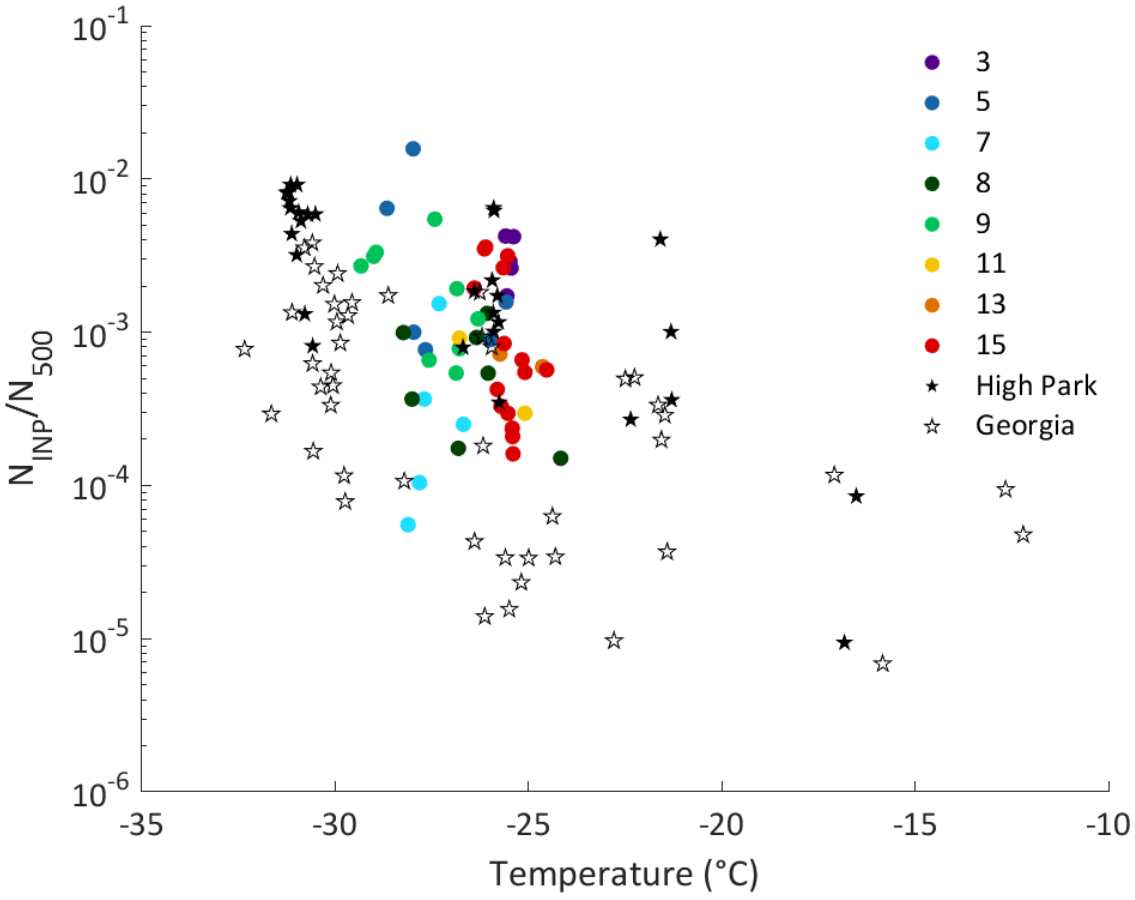

Figure 3.4. The ratio of N_{INP} to N_{500} (CFDC data only) for the eight cases analyzed from the WE-CAN campaign (filled circles) and the High Park wildfire (filled stars) and Georgia prescribed burn (open stars) data from McCluskey et al. (2014).

3.2.2. Surface Active Site Density Parameter

The surface active site density parameter (n_s) normalization, which allows for comparison between fires analyzed during the WE-CAN campaign for both the online data from the CFDC and filter collections analyzed with the IS and to other known sources of INPs, is shown in Figure 3.5. It is important to mention that this parameter is not plume-background subtracted, but rather includes everything sampled in the plume, since RF5 and RF8 sampled aged smoke without a definable "background" period, and some uncertainty exists in quantification of background IS filters where not enough volume of air was collected (more details in Section 3.3). Therefore, the assumption in this normalization is that the surface area of aerosols from the PCASP and the INPs are all unique to the plume, which shown in Sections 3.2.3 and 3.3, is reasonable for some but not all fires for INPs.

The exponential fits from Ullrich et al. (2017) for desert dust (measured in the laboratory) and from McCluskey et al. (2018) for sea spray aerosols in clean marine air are plotted for comparison to the plume data. The n_s for biomass burning aerosols from WE-CAN is approximately 3 orders of magnitude lower than the dust fit, but similar to the clean marine INP fit for data obtained in the North Atlantic. This is not unexpected as McCluskey et al. (2014) found a low fraction of ice nucleating particles in wildfires to total aerosol larger than 500 nm, but in comparison to a good ice nucleator like dust, wildfire smoke is an inefficient source of INPs. This does not imply that smoke and clean marine air masses have the same overall INP concentrations since the airborne surface area of smoke aerosols is much larger than that for marine aerosols, at least until the smoke is heavily diluted. Among WE-CAN fires, there is some variability in n_s, but all show an increase with decreasing temperature. The Taylor Creek (RF3)

and Donnell (RF7) fires have the lowest n_s out of the investigated fires, almost five orders of magnitude lower than desert dust at -25 °C. Table 3.4 gives the average surface areas from the PCASP during both the CFDC and IS plume sampling times, and shows the Donnell (RF7) fire having the largest surface area for all IS filter collections, while the largest average surface area during CFDC sampling comes from the Mendocino Complex fire in RF13. Figure 3.5 highlights the INP variability between fires as there is low n_s for both the Donnell (RF7) and Taylor Creek (RF3) fires, but they have significantly higher and lower aerosol surface areas respectively. The River of Smoke (RF5) and South Sugarloaf (RF15) fires have CFDC points that are the highest of the n_s values from WE-CAN, despite the filter collection n_s not being exceptionally high. The elevated n_s values from RF5 also coincide with the higher ratios from normalizing with N_{500}. This variability reflects the heterogeneity in particle loading and INP concentrations although smoke is an inefficient ice nucleator in all cases.

The filter collections additionally demonstrate that n_s can vary strongly as a function of temperature, as the Taylor Creek (RF3) fire has a comparable n_s to other fires at the warm end of the temperature spectrum (>-20 °C), followed by a lower n_s at lower temperatures before joining up with the rest of the filters and CFDC points at the coldest part of the spectrum. These trends likely arise because different particle types dominate the INP spectra in several temperature regimes, as seen in Figure 1.4, and different fires emit different proportions of these various types. Possible particle identity will be discussed in detail in Section 3.3, but INPs are likely primarily organic material, with the potential of lofted wood ash from biomass burning fuels to nucleate at the coldest end of the temperature spectrum based on previous laboratory studies. Grawe et al. (2016) found wood ash to nucleate below -35 °C, and could be

a potential INP source, but no measurements were made in WE-CAN at this temperature. However, Umo et. al (2015) parameterized a wood ash fit for n_s that is valid up to -11 °C, which looks similar to some of the higher CFDC points at the cold end of the temperature spectrum and will be explored in greater detail in future efforts.

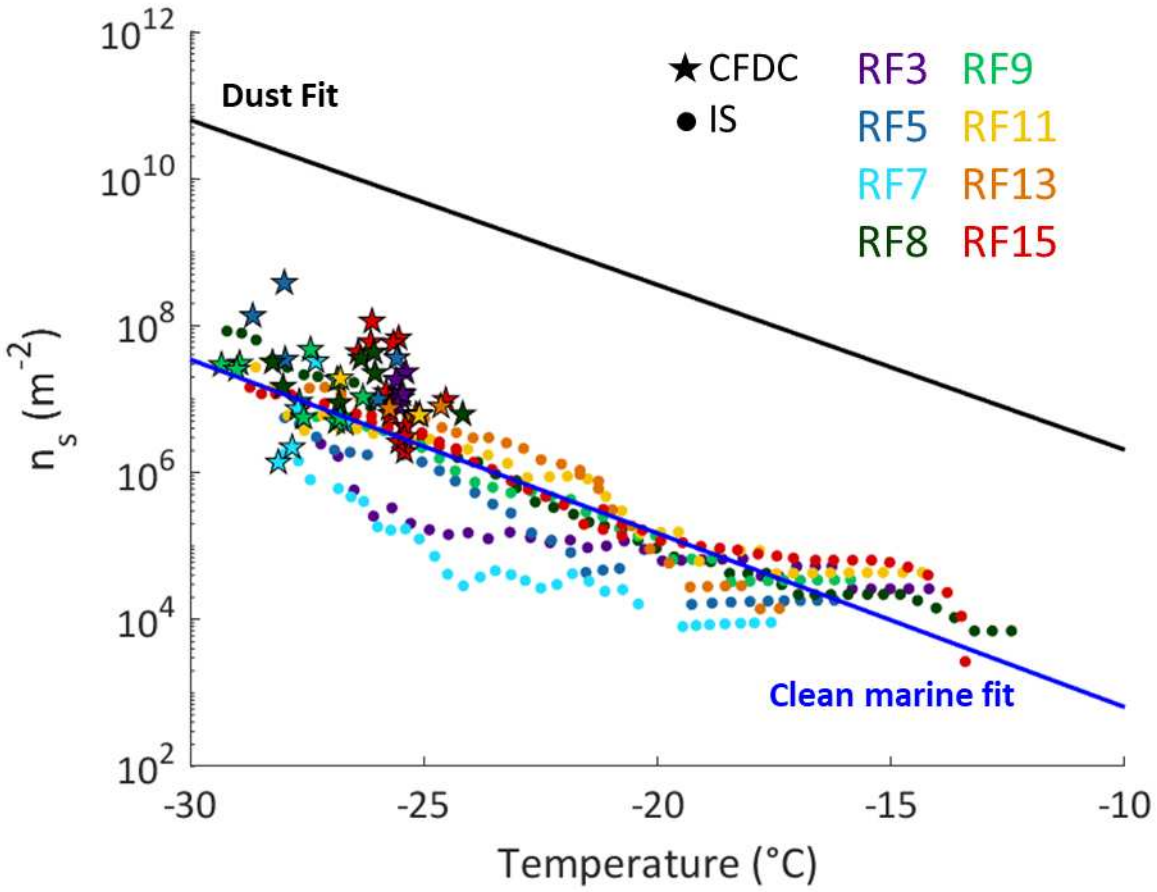

Figure 3.5. INP surface active site density parameter (n_s) for the filters analyzed with the IS (circles) and CFDC plume passes (stars), colored by fire. Fits from previous work are shown in solid lines for comparison to the WE-CAN campaign (dust fit from Ullrich et al. (2017) in black and clean marine fit from McCluskey et al. (2018) in blue).

Table 3.4. Average surface area (A) from the PCASP (under 2.5 μm) during the CFDC and IS plume sampling times.

Flight	Average A CFDC ($\mu m^2 cm^{-3}$)	Average A IS ($\mu m^2 cm^{-3}$)
3	2522	1762
5	497	571
7	2196	3419
8	616	527
9	1173	722
11	658	404
13	3476	1581
15	2472	2077

3.2.3. Normalized Excess Mixing Ratio

The results from the NEMR calculations, which provide a way to analyze INP concentrations after accounting for plume dilution, are focused in this section. The INP backgrounds from the fires for calculating NEMR, as measured by the CFDC, are shown in Table 3.5. All of the backgrounds are relatively clean, with the Taylor Creek (RF3) fire having the lowest background INP concentration, while the Bear Trap (RF9) fire has the highest background INP concentration. Figure 3.6 compares the calculated background INP concentrations with their respective plume passes and illustrates that the background for an individual fire is lower than almost every associated plume pass, with the exception of two passes in the Bear Trap (RF9) fire. However, background concentrations are almost always within an order of magnitude of the plume passes, with some notable exceptions in the Taylor Creek (RF3) and South Sugarloaf (RF15) fires. Since only CFDC data are used in NEMR calculations from having higher temporal resolution data, the out-of-plume background data from the IS will be discussed in Section 3.3.

Table 3.5. CFDC INP background concentrations for the 6 fires used in NEMR calculations. As explained in the methods, one background value was used for each fire.

Flight	CFDC INP Background (L^{-1} STP)	Temperature (°C)
3	1.1	-25.5
7	3.7	-27.6
9	11.1	-28.2
11	3.5	-25.2
13	7.7	-25.7
15	4.5	-25.5

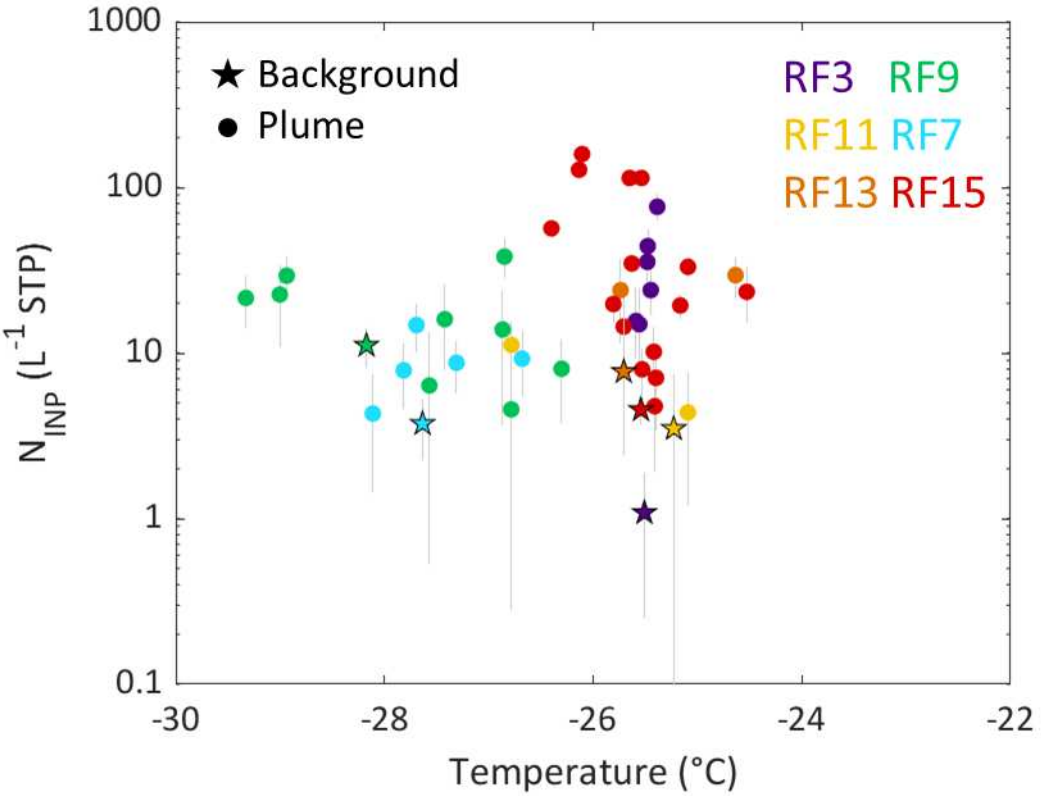

Figure 3.6. CFDC INP plume concentrations (circles) and their associated out of plume background (stars) for the 6 fires for which NEMR analysis was conducted. Error bars indicate 95 percent confidence intervals.

Figure 3.7 shows the results of the NEMR calculations as a function of plume age from the six smoke plumes analyzed. Sampling strategies resulted in plume ages on the order of a few hours, with the majority of points under two hours. Most fires have passes with low NEMRs

that stay relatively constant in time (under 0.1 $L^{-1}ppb^{-1}$ shown in the light gray box), but there is still variability, with the greatest exceptions from the South Sugarloaf (RF15) and Bear Trap (RF9) fires. This may indicate that there are other processes happening within the plume, such as dissimilar sources of INPs within the overall smoke plume being lofted up at different times or possible in-plume production of INPs. McCluskey et al. (2014) found tarballs in a TEM grid collected from the High Park fire. TEM grids from WE-CAN will be analyzed in the future to see if this was evident during these cases indicating INP production.

To our knowledge, the results here are the first attempt to use in situ, free tropospheric data to characterize the NEMR for INPs. With the majority of NEMRs constant in time, this approach could be used in modeling studies that track the transport and dispersion of various aerosol species to predict the background-subtracted INP emissions from wildfires based on modeled CO emissions. There is promise in this calculation, especially in the Taylor Creek (RF3) and Donnell (RF7) fires that have several plume passes with various ages and have relatively constant NEMRs. Global modeling studies tagging different sources of INPs could then be used to compute the relative contributions of each source to observed INPs at any location in the atmosphere. Since most of the INP data from WE-CAN were collected over a narrow temperature range, the slope of the n_s fits could be applied to NEMR for insight into temperature dependence, assuming similar decay rates. This method and application will be explored in greater detail in the future.

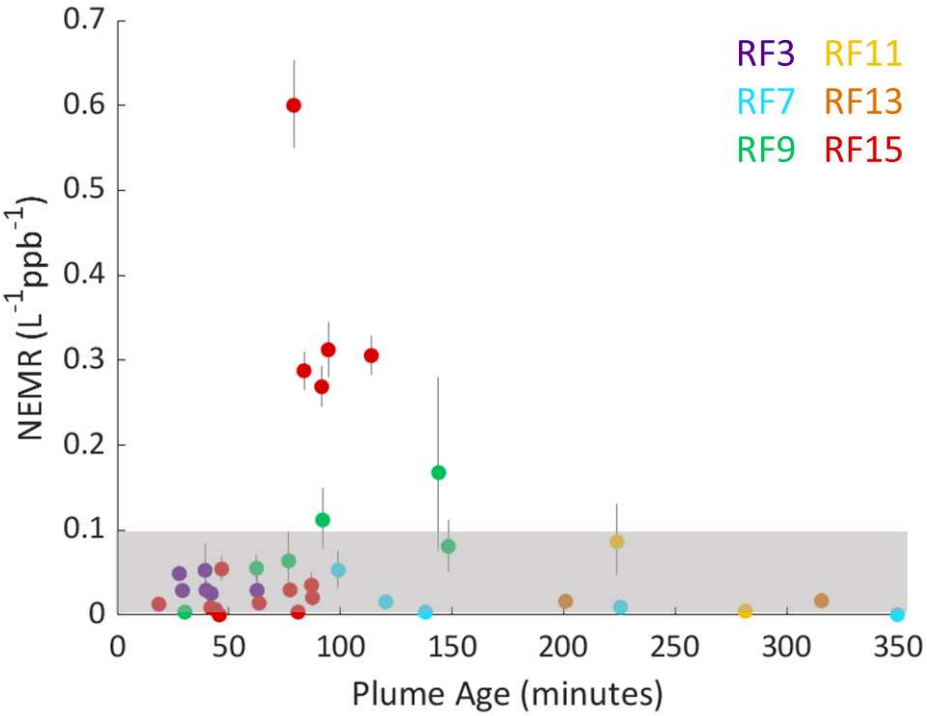

Figure 3.7. INP Normalized Excess Mixing Ratio (NEMR) as a function of plume age, colored by fire. The light gray box is drawn for NEMRs under 0.1 $L^{-1}ppb^{-1}$. 95 percent confidence intervals are shown in gray.

3.2.4. Urban Influences on INP Concentrations

The iso- to n- pentane ratios were calculated for all CFDC plume periods to test for correlations between urban influence and smoke. These calculations were only made on the CFDC data for analysis at shorter timescales. Figure 3.8 confirms that the highest ratios were observed during RF8 sampling the Central Valley boundary layer, with elevated ratios also present in the River of Smoke (RF5) and Bear Trap (RF9) fires, confirming some urban influence in a number of sampling flights. Previous studies have found that biomass burning has an i:n pentane ratio of approximately 0.5 (Simpson et al. 2011), and this fits well with the majority of the fires studied during WE-CAN.

The data in Figure 3.8 show that there is no correlation between the INP number concentrations and the i:n pentane ratio, as the highest and some of the lowest concentrations are during the South Sugarloaf fire of RF15, which had little to no urban influence. In RF8, there were similar INP concentrations throughout (within an order of magnitude), even though there were varying degrees of urban influence. To normalize the INP concentrations, the surface active site density parameter (n_s) was also plotted against the i:n pentane ratio in Figure 3.9, highlighting the scatter and variability among fires in the number of ice-nucleating sites per surface area of smoke with increasing urban influence. Therefore, no strong evidence was found in the WE-CAN dataset to support a relation between INP concentrations and degree of urban influence, at least when using isopentane as a tracer. This suggests that even though urban INP sources may exist, they exert little regional impact on the INP budget when smoke is present (and possibly even when it is not).

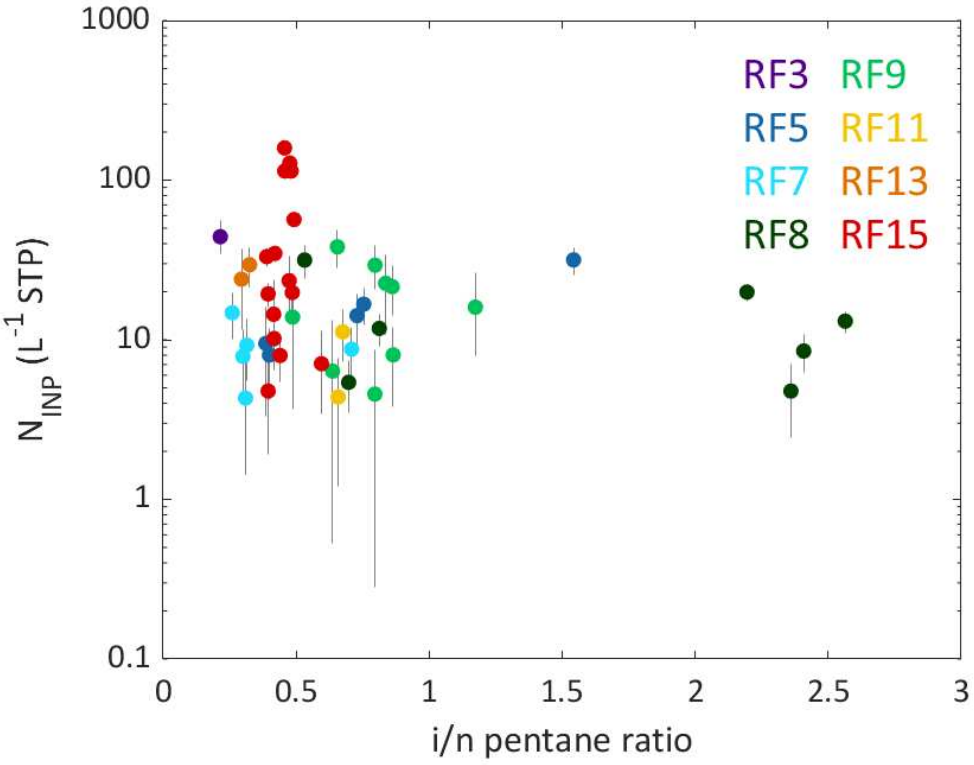

Figure 3.8. INP number concentrations as a function of the iso- to n-pentane ratio for the 2 aged smoke cases (flights 5 and 8) and the 6 smoke plumes analyzed. The 95 percent confidence intervals for N_{INP} are given in gray.

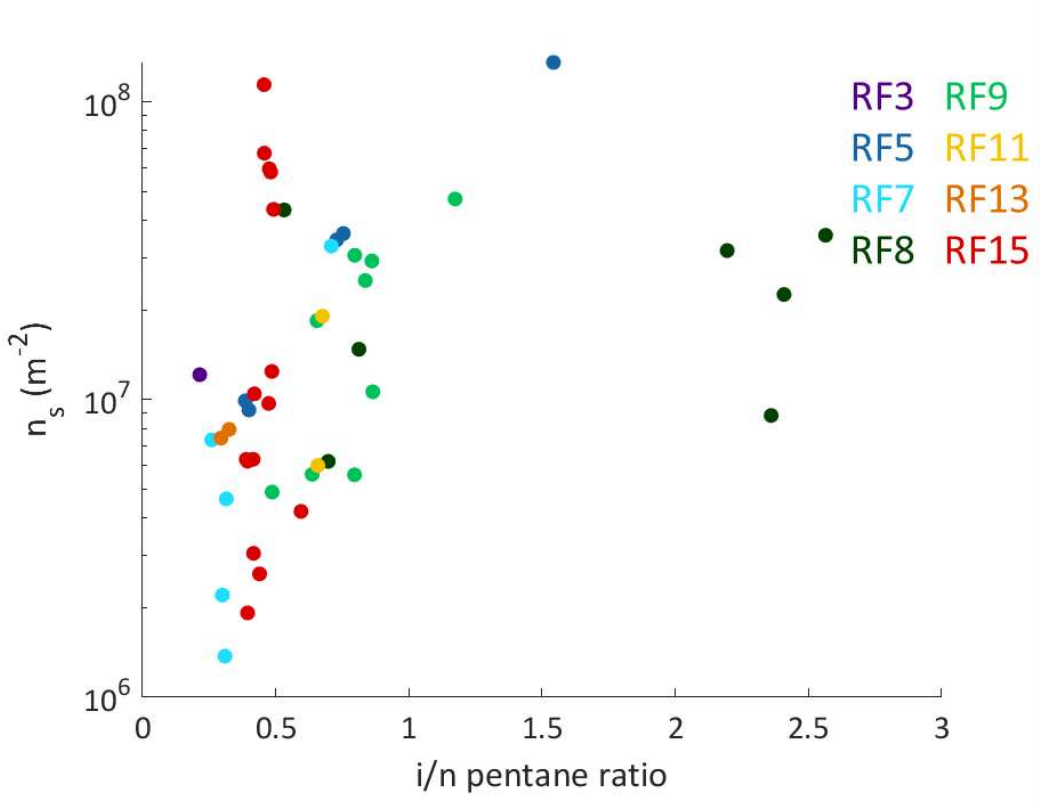

Figure 3.9. INP surface active site density parameter (n_s) as a function of the iso- to n-pentane ratio for the 2 aged smoke cases (flights 5 and 8) and the 6 smoke plumes analyzed.

3.3. Ice Spectrometer-Focused Results

This section presents an overview of all ice spectrometer data and results of the heat and peroxide treatments to answer the question of what composition the INPs released from the wildfires are. First, an example of how the INP temperature spectra for the plume versus its background air compare is shown in Figure 3.10. The Taylor Creek (RF3) fire out-of-plume background has no detectable points after blank filter corrections, despite having a lower limit of detection from a larger volume of air filtered than the plume filter. This implies that more volume of air would have had to be collected to have a detectable INP temperature spectrum, but this was not possible with the sampling strategy of the aircraft. The Donnell (RF7) fire has a different structure where at the warm end of the spectrum (>-20 °C), the plume and

background air are similar (though with high uncertainties), but the colder end has no detectable INPs in the background. Figure 3.10 also highlights the variability between the plume and background filters in when the wells start freezing in the IS, as the Taylor Creek (RF3) fire background does not start freezing until -22 °C (below the limit of detection), while the Donnell (RF7) fire background INPs are detectable for freezing at about the same temperature as the plume filter.

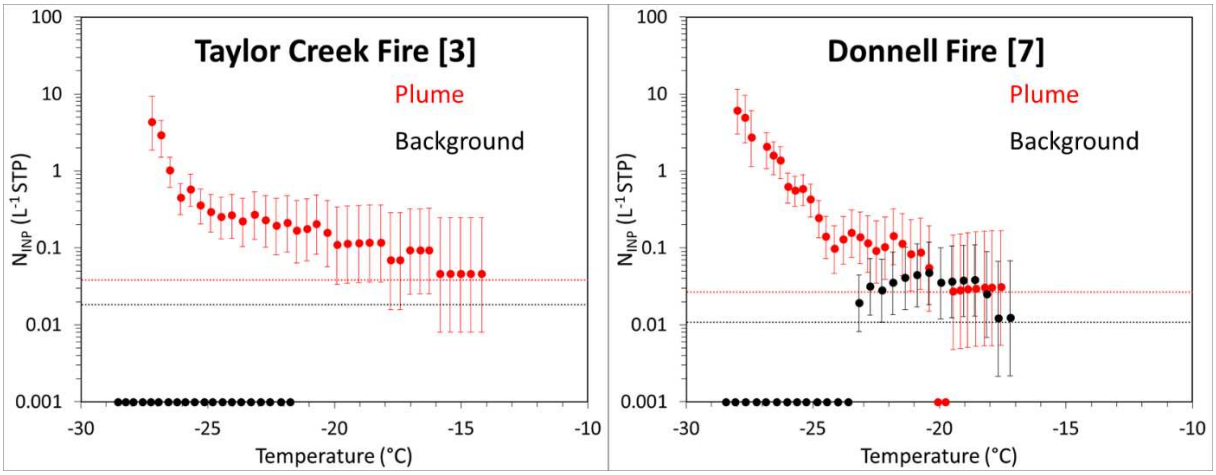

Figure 3.10. INP temperature spectra for the plume (red) and out-of-plume background air (black) for the Taylor Creek (RF3; left) and Donnell (RF7; right) fires. Points below the limit of detection (dashed lines) are given default values of 0.001 L^{-1}.

Compiling all detectable filter measurements that were analyzed with the Ice Spectrometer (IS) is a generalized way to compare plume measurements with out-of-plume background air (Figure 3.11) and see if plumes can be a source of INPs. Although from Figure 3.11, it may appear that there is little change in the INP number concentration spectra between plume and background filters, it is evident that background definition is strongly dependent on an individual fire. One of the prominent takeaways from this figure is that most detectable INPs at temperatures warmer than about -20 °C were only from in-plume measurements. This does not imply that there are no INPs in the background air at warmer temperatures, rather that, for

the sample volumes collected, number concentrations in out-of-plume air rarely exceeded the detection limit of the IS, whereas in plumes they oftentimes did. The other main point is that the majority of the lowest INP concentrations are from the background filters, while the majority of the highest INP concentrations come from in plume collections. From Figures 3.10 and 3.11, there are normally elevated INPs in the plume air compared with its background, but this is not necessarily at all temperatures of the spectra and the magnitude is heavily fire-dependent.

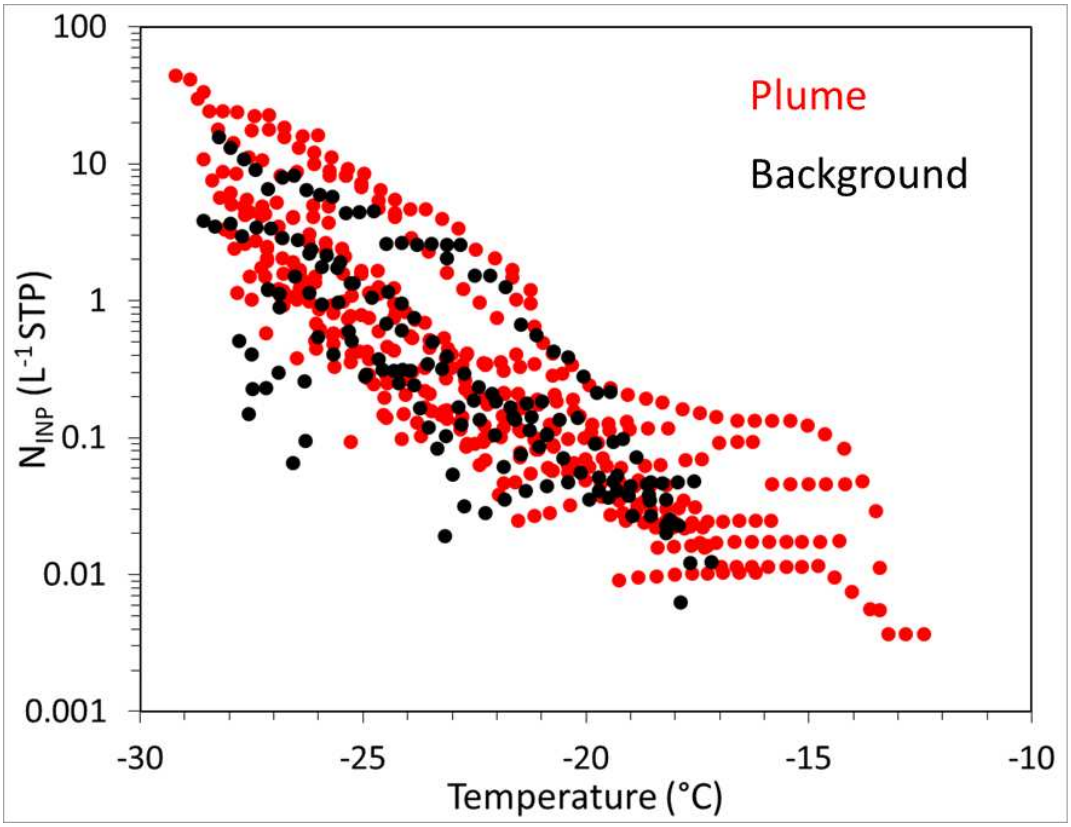

Figure 3.11. INP cumulative number concentration spectra composite plot for both in plume (red) and out-of-plume background (black) filters analyzed with the CSU Ice Spectrometer (IS). Concentrations for background filters were below detection limit for temperatures warmer than -17 °C.

Treatments were done on the remaining liquid suspensions for several filters to obtain additional information on possible compositions of the INPs. The combined results are

presented in Figure 3.12. Filters with only enough suspension remaining to perform the peroxide digestion are shown in Figure 3.13. The Donnell (RF7), Taylor Creek (RF3), and Mendocino Complex (RF13) fires have noticeable changes after heating and therefore have a large biological component. The River of Smoke (RF5) and Shellrock (RF11) fires have no difference in their spectra after heating, so the biological fraction is small. Digestion with hydrogen peroxide and UV-B light removes organics in the original sample. Results from this treatment indicate a significant heat-stable, but organic influence in all smoke samples tested. This is evident at all ends of the temperature spectrum, including in the temperature region where mineral INPs are thought to dominate (i.e., below -15 °C; Murray et al. 2012). Peroxide digestion removed almost all of the INPs from the Taylor Creek (RF3) and Donnell (RF7) fire smoke samples, indicating the significance of organic INP populations. Comparing the two treatments reveals that the Shellrock fire (RF11) and River of Smoke (RF5) have few heat-labile organic INPs but have a large heat-stable INP population, whereas the other fires have variable levels of both heat-labile and stable INP populations. The Mendocino Complex fire filter (RF13) is particularly interesting as the influence of organic INPs is most prominent at the cold end of the temperature spectrum. The blue diamonds from the peroxide treatment that decrease with colder temperatures is an artifact of little freezing (a plateau) at these temperatures while INPs in the field and peroxide blanks go up monotonically with lower temperatures. Therefore, for clearer interpretation, the INP temperature spectrum without blank correction is plotted in open blue circles. The open circles are consistent with the possibility of a larger organic influence at the coldest temperatures, which could be from a different sub-population of smoke INPs that were more impacted from peroxide digestion. The results of the treatments

still indicate a mineral presence in the plume filters tested from WE-CAN from detectable INPs remaining after peroxide digestion in a number of filters, but the conclusion here is that organics made up a significant proportion of the total plume INPs sampled. INPs from soils cannot be ruled out as arable soils have been shown to have organic INPs (Tobo et al. 2014; Hill et al., 2016), but the pure mineral influence is generally small.

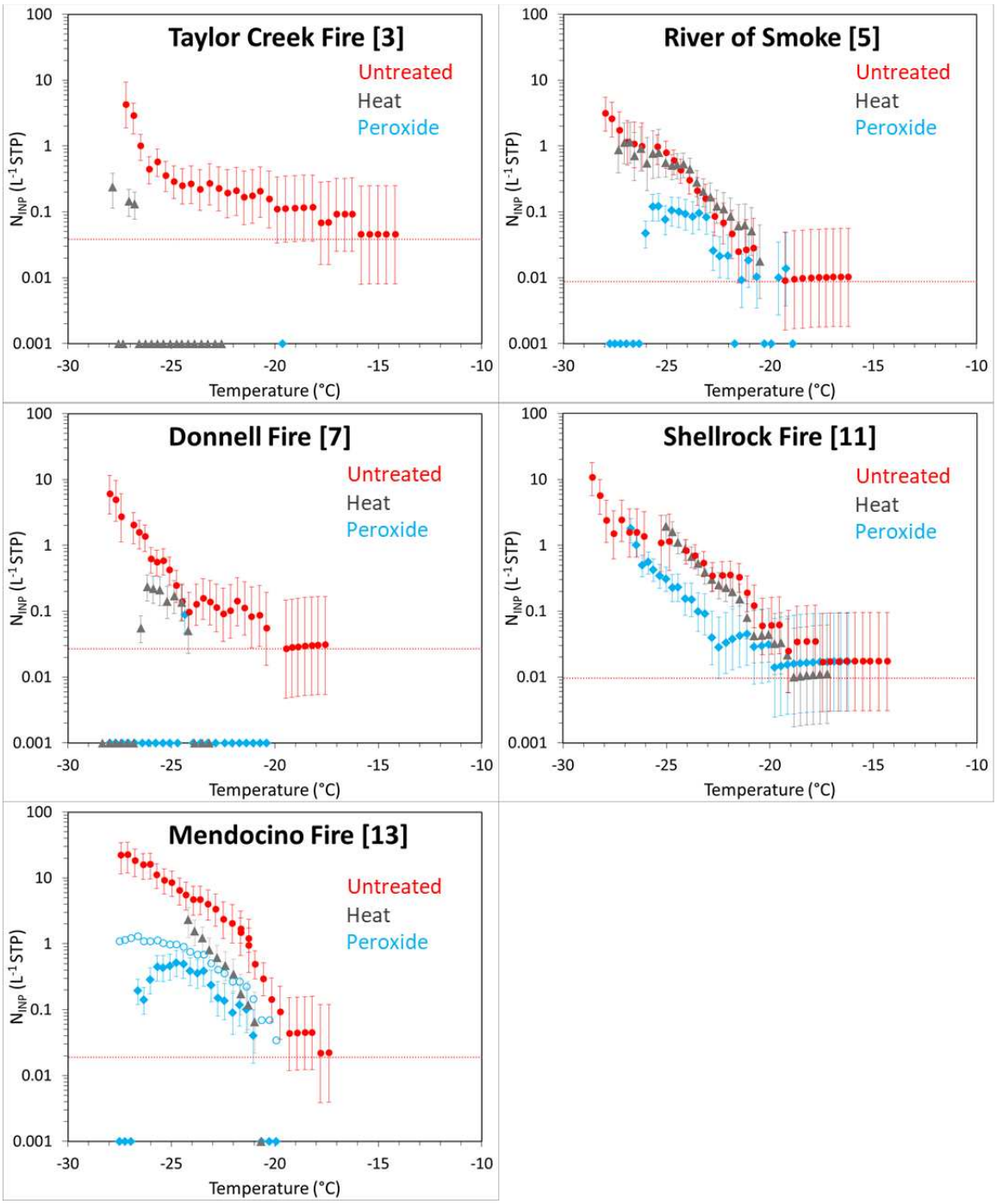

Figure 3.12. Heat and peroxide treatment results on selected smoke filters, with red circles showing untreated INP temperature spectra, gray triangles showing spectra after 20 minutes of heating at 95 °C, and blue diamonds showing spectra after 20 minutes of digestion with hydrogen peroxide and UV-B light. Below the limit of detection data in the heat and peroxide treatments are given default values of 0.001 L^{-1}. Limit of detection is plotted as a red dashed line for each sample. The blue open circles for RF13 show values after peroxide digestion uncorrected for blank filters.

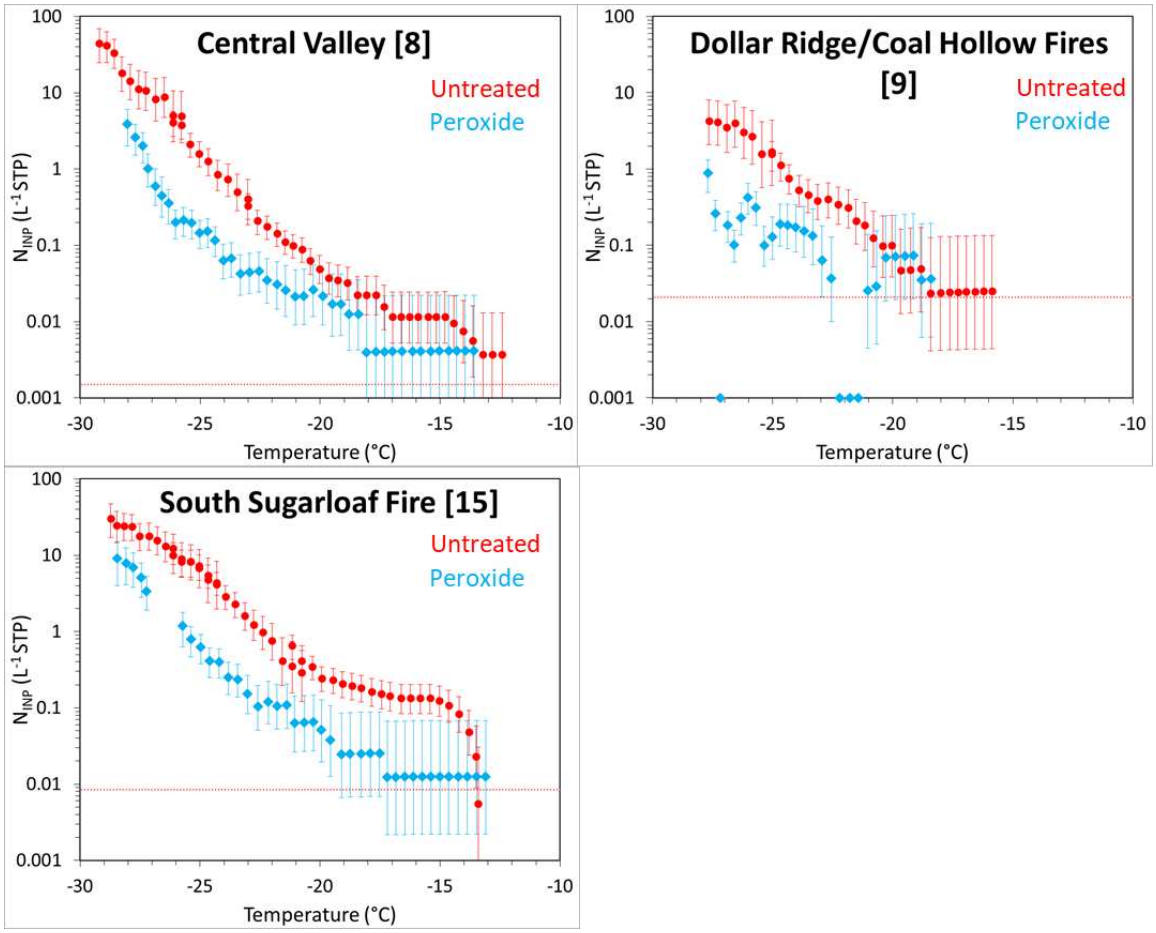

Figure 3.13. Peroxide treatment results on select smoke filters, with red circles showing untreated INP temperature spectra and blue diamonds showing spectra after digestion with hydrogen peroxide and UV-B light for 20 minutes. Below the limit of detection data in the peroxide treatments are given default values of 0.001 L^{-1} and the limit of detection is plotted as a red dashed line.

3.4. Comparison Between the CFDC and IS for Plume Measurements

In this section we look in more detail at two of the flights shown in the INP composite plot (Figure 3.3) to elucidate reasons for differences in the "point" (integrated only over one plume pass) measurements (CFDC) and flight-integrated filter-based measurements (IS). Figure 3.14 illustrates a case from the Central Valley flight where the CFDC and IS agree relatively well, with several CFDC points right on top of the INP temperature spectrum from the IS and nearly

all CFDC points are within a factor of 2 of the IS data. In contrast, Figure 3.15 shows that most of the CFDC plume-pass INP concentrations in RF15 are higher than the IS data, with the highest concentrations of over 100 L^{-1} being over a magnitude larger. One of the reasons for discrepancy is due to the differing time resolutions for the two methods. When an aerosol filter is collected, it needs several minutes at a minimum to resolve INP concentrations above the detection limits determined on the basis of blank filters. The CFDC can generally resolve individual plume passes. Furthermore, due to each pass not being the same number of seconds, a shorter (but still statistically significant) pass with large INP concentrations on the CFDC may be a minute part of the total volume of air collected on a filter for the IS.

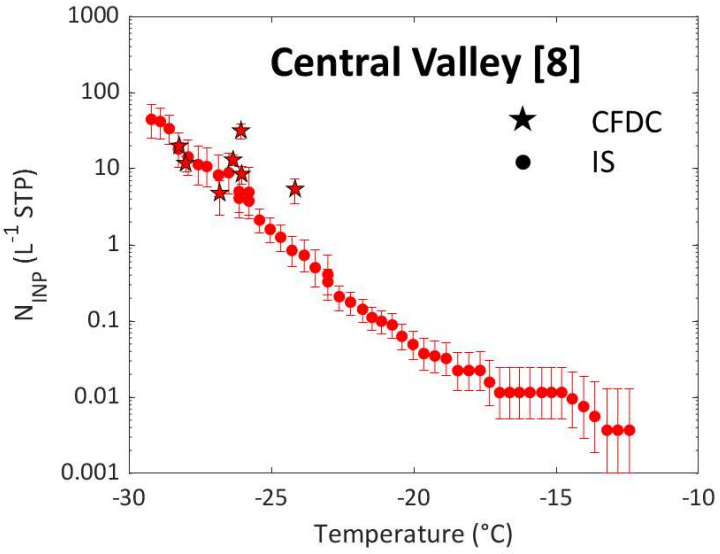

Figure 3.14. Comparison between the INP temperature spectra from the IS (circles) and sampling periods from the CFDC (stars) for the sampling of the Central Valley boundary layer in RF8.

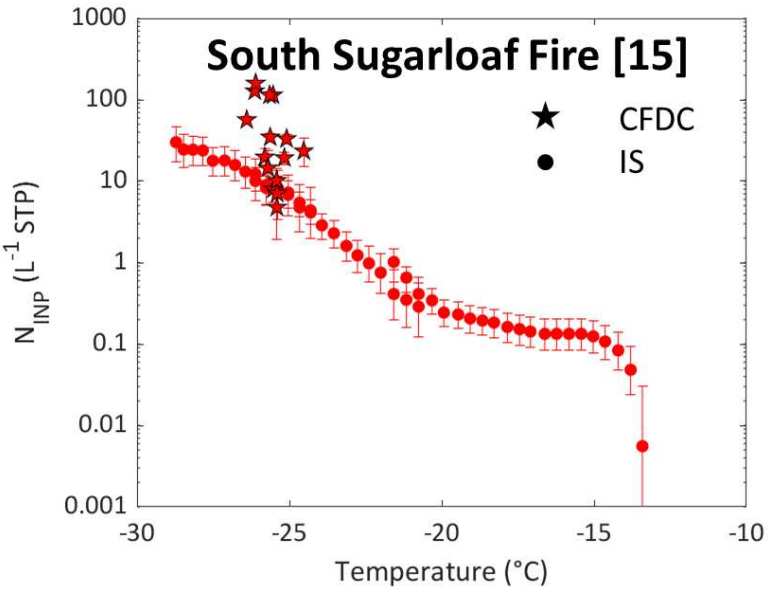

Figure 3.15. Comparison between the INP temperature spectra from the IS (circles) and sampling periods from the CFDC (stars) for the South Sugarloaf fire in RF15.

Although the CFDC has higher temporal resolution in INP concentrations when compared to the IS, it still has much lower temporal resolution than many instruments on the aircraft that have 1 Hz measurements. To investigate what a plume pass would look like for INP concentrations on these timescales, raw ice counts were plotted for the South Sugarloaf (RF15) fire by summing over all the ice bins but not correcting for instrument filter backgrounds. Figures 3.16 and 3.17 distinctly show the majority of ice counts are in the center of the plume and decrease toward the edges. This is important when analyzing and interpreting the INP concentrations of plumes, as they might be much higher at shorter timescales and smaller spatial scales, but the relatively low numbers of INPs sampled in the free troposphere limit the possibility of subdividing the defined plume passes further here but will be explored in future work.

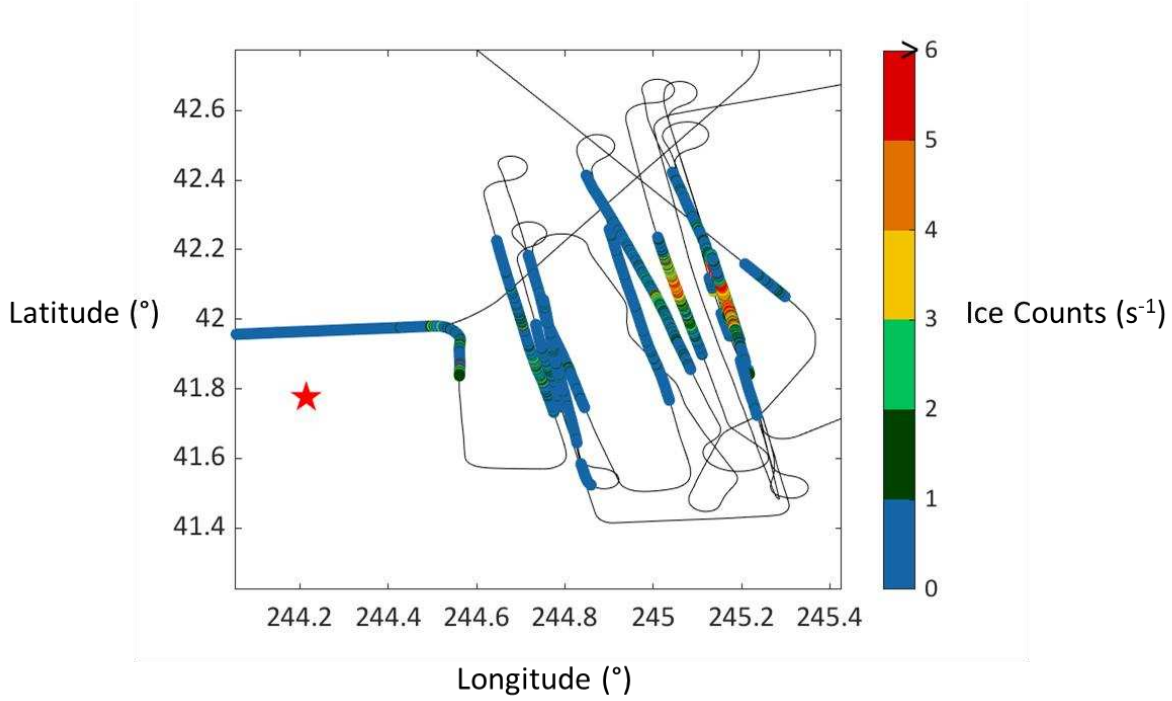

Figure 3.16. Two-dimensional one second uncorrected ice counts during plume passes for the South Sugarloaf (RF15) fire, with the red star depicting the fire center.

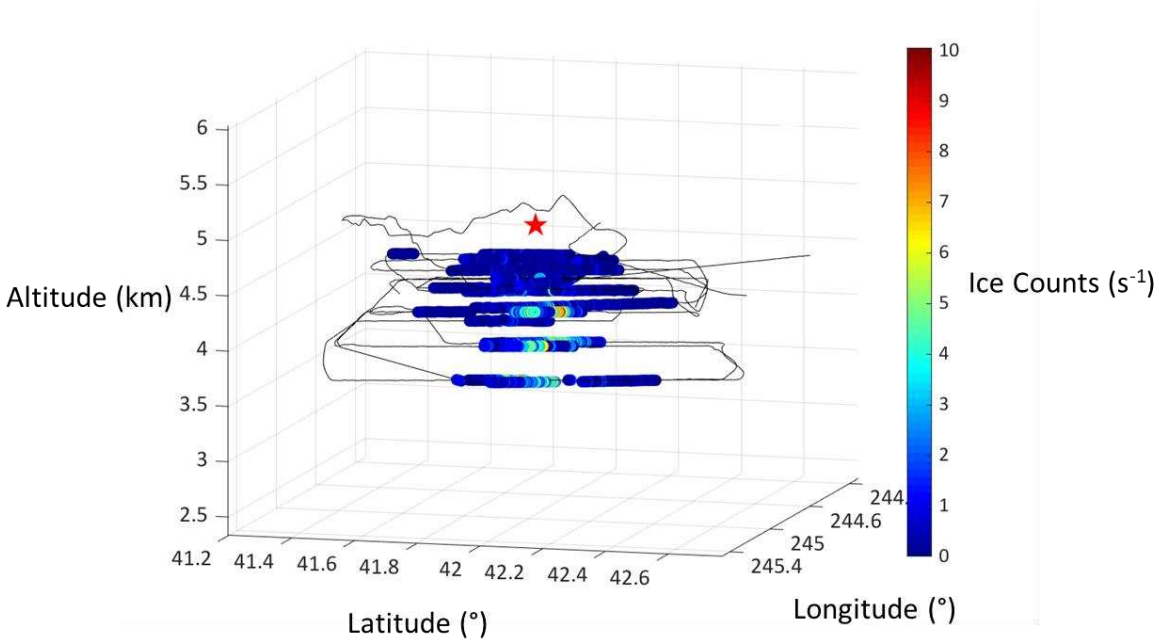

Figure 3.17. Three-dimensional one second uncorrected ice counts during plume passes for the South Sugarloaf (RF15) fire, with the red star depicting the fire center.

3.5. Case Study: South Sugarloaf Fire

One of the best sampling periods for the CFDC occurred during RF15, which probed smoke from the South Sugarloaf fire on August 26, 2018, due to the sampling design that included multiple cross-plume passes at several altitudes. The predominant fuel type burned was sagebrush shrubland (with Aspen forest interspersed). Soil and plant tissue from this ecosystem have previously been tested for INP properties (Schiebel et al., 2017; Hill et al., 2016). As illustrated in the previous figures in this chapter, INP concentrations measured in RF15 were often much higher than data from other plumes that tended to cluster more closely in both unnormalized and normalized presentations. There was also a large organic INP influence at all temperatures inferred from the decrease after peroxide digestion (Figure 3.13). Figure 3.18 presents a four-dimensional picture of the CFDC INP measurements for this flight. The largest INP concentrations were observed in the lower altitude passes further away from the fire center (red star shows latitude and longitude). In Figure 3.19, these same data are shown as functions of plume age, demonstrating generally that the highest INP concentrations at several altitudes had greater plume aging. Concentrations exceeded over 100 L^{-1} during some passes, which is unusual for any other fire sampled during WE-CAN, and unexpected given this flight was near the end of the campaign.

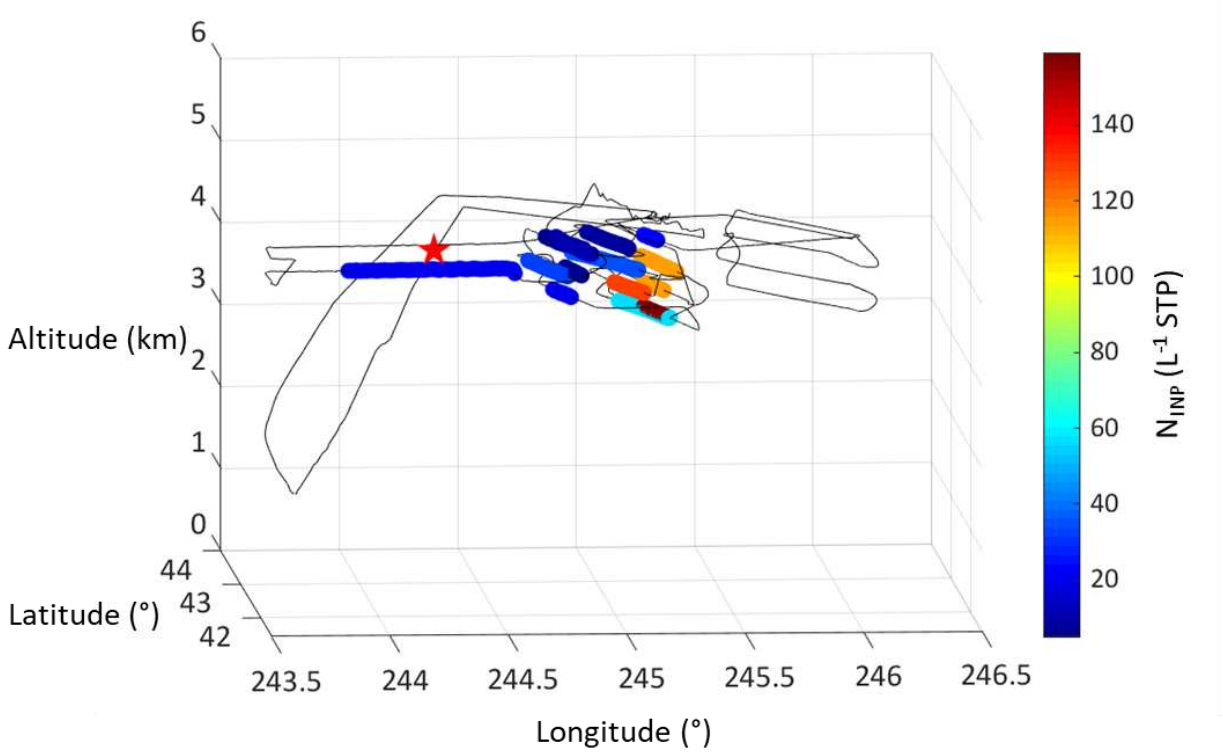

Figure 3.18. RF15 flight track, with the South Sugarloaf fire passes captured by the CFDC colored by INP concentration. The red star indicates the fire center latitude and longitude.

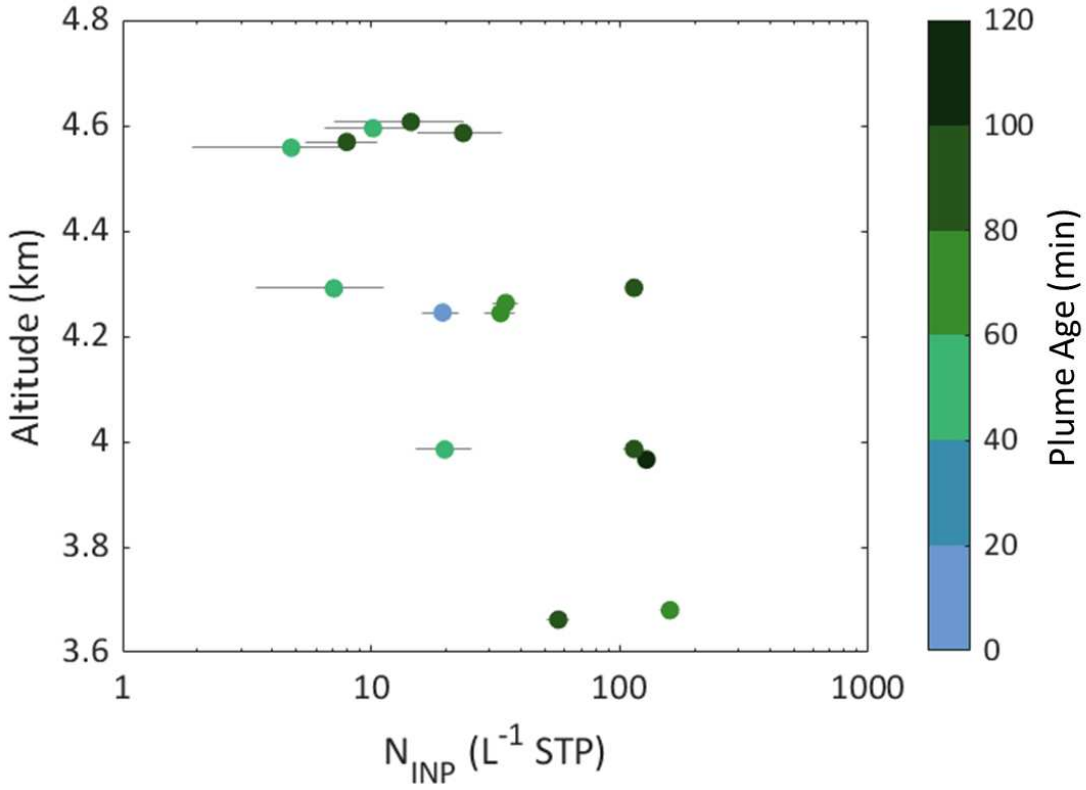

Figure 3.19. Average altitude above sea level (in kilometers) as a function of CFDC INP concentration for the South Sugarloaf fire passes. Points are colored by plume age (in minutes) and 95 percent confidence intervals on N_{INP} are in gray.

The question then becomes what is special about this fire and its atypical INP properties. Figure 3.20 shows the INP temperature spectra from both the plume and its associated background air. The enhanced concentrations and warmer limit of detection in the plume relative to the background are consistent with the general conclusions drawn from the composite plot (Figure 3.11). However, the shape of the RF15 plume INP temperature spectrum is unique and does not resemble the out-of-plume background INP spectrum. When including the results of peroxide digestion on the plume filter (Figure 3.21), the spectrum looks similar to the background filter in shape and magnitude, and its warm temperature hump is removed. This is evidence for the plume contributing organic INP populations that the aircraft sampled, and peroxide treatment on the background filter could be done as verification to this hypothesis. Additionally, the presence of a warm temperature hump has been seen in previous work that suggests a biological INP presence (Hill et al., 2018). Hill et al. (2016) showed this structure in the soils tested that had both heat-labile and dominant heat-stable INP populations, while Suski et al. (2018) found this characteristic of a large presence of heat-labile organic INPs released from crops.

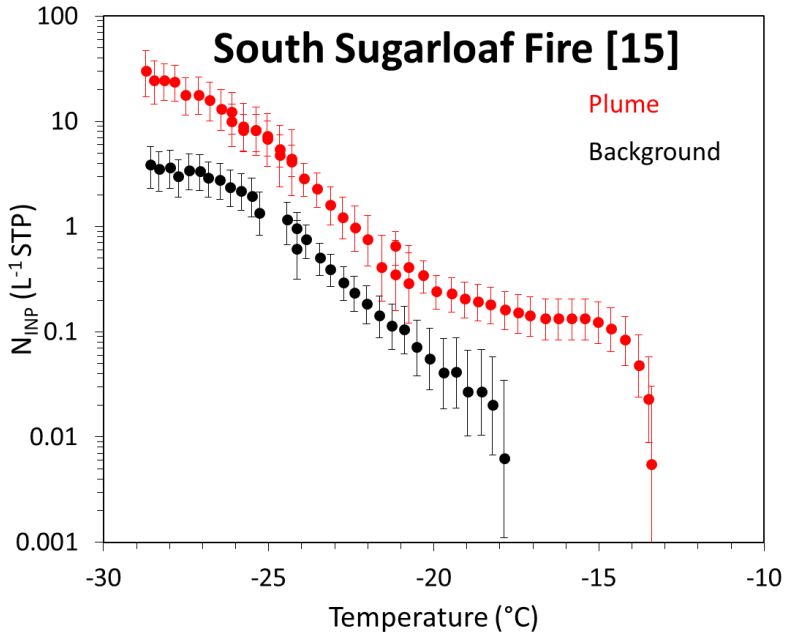

Figure 3.20. South Sugarloaf fire INP temperature spectrum for the plume in red and out-of-plume background air in black for the filters analyzed with the IS.

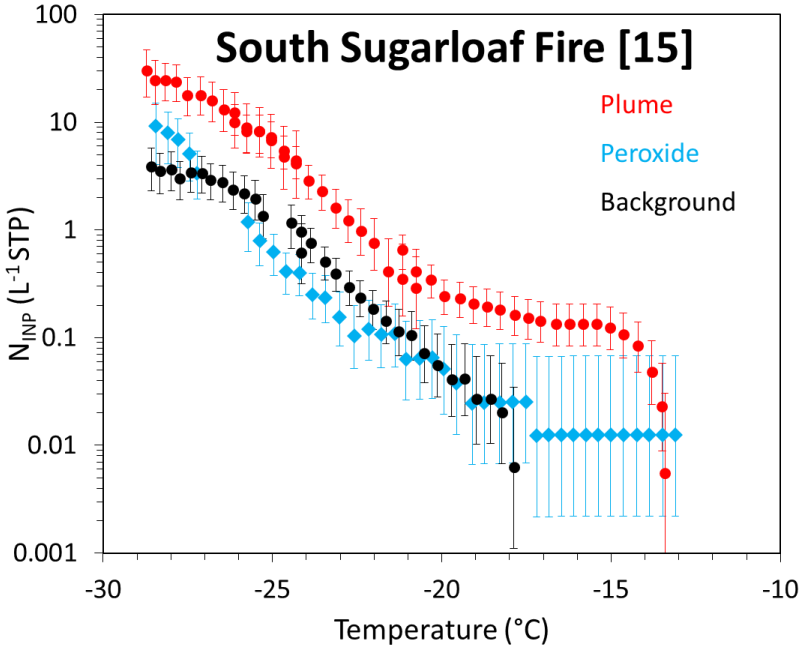

Figure 3.21. South Sugarloaf fire INP temperature spectrum for the plume in red, peroxide treatment on the plume filter in blue, and out-of-plume background air in black for the filters analyzed with the IS.

Based on the evidence of organic INPs lofted into the South Sugarloaf fire, the potential role of INPs in soil versus what is released from vegetation was investigated. Sagebrush (Artemisia tridentata) clippings from near Woods Landing-Jelm, Wyoming were taken from approximately 30 different shrubs. This is the same site (Figures 3.22, 3.23) from which soil samples were taken and analyzed for INP properties in 2015 (Thea Schiebel, unpublished). Clippings were put into a 1-gallon plastic slider bag and filled approximately half of the bag. These bags have been tested with the IS to show almost no contributions from the bags themselves to INPs across the temperature spectrum of the instrument. The sagebrush clippings were then taken back to CSU, shaken for 5 minutes (to simulate fire-driven turbulence) followed by waiting 10 minutes to allow aerosolized particles to settle (Figure 3.24). All of the clippings were then removed from the bag, and 20 mL of DI water was added to resuspend the particles and placed into a clean 50 mL centrifuge tube for analysis with the IS. Another 1-gallon bag of sagebrush clippings was taken and shaken for 5 minutes with 200 mL of DI water for comparison to the dry-released INPs. Both units are in per gram of fresh weight vegetation, shaken and washed respectively.

Figure 3.22. Location of previously tested sagebrush soil and where sagebrush clippings were taken in 2019.

Figure 3.23. Picture of the site near Woods Landing-Jelm, Wyoming, where sagebrush was sampled.

Figure 3.24. Two sagebrush collection bags that were analyzed with the IS for INP properties.

Figure 3.25 presents the results of the test. The INP temperature spectra from the aerosolized sagebrush and the aircraft filter have striking similarities. They both have a similar inflection point around -21 °C (black box drawn), but they also show a rapid increase in INP concentration between -13 and -14 °C, with nearly identical slopes, indicating an onset of an INP population at the same temperature. This increase is not present in the tested soil dust. The aerosolized sagebrush has another population of INPs at temperatures warmer than -13 °C that the aircraft filter would not be able to see due to the limit of detection of the IS. These results suggest the presence of dry-dislodged sagebrush INPs that were collected in the aircraft filter. This is likely a mixture of dust and biological plant material that are on the leaves. Although the filter was taken over a different area and year, all samples were collected within a month of each other seasonally and sagebrush is heavily present throughout the Western U.S. so similar INP properties can be expected. This does not mean that the sagebrush soil and other fuels that comprised the fire had no impact, but the findings suggest that what is on the shrubs can have a dominant influence on the INP population in the atmosphere (at least locally) and were likely lofted into the plume. Figure 3.25 also shows that the washed sagebrush clippings have similar INP properties to the dry shaking and aircraft filter, with the characteristic onset near -13 °C and presence of warm temperature INPs. Moreover, Figure 3.26 illustrates the comparisons between the aircraft filter and aerosolized sagebrush when scaling the sagebrush INP spectrum by 500,000. It is not expected that these spectra would line up perfectly given the free tropospheric plume sampling with an inlet versus ground-derived shaking, but this figure shows the nearly identical onset of an INP population at -13 °C and similar inflection point at -21 °C.

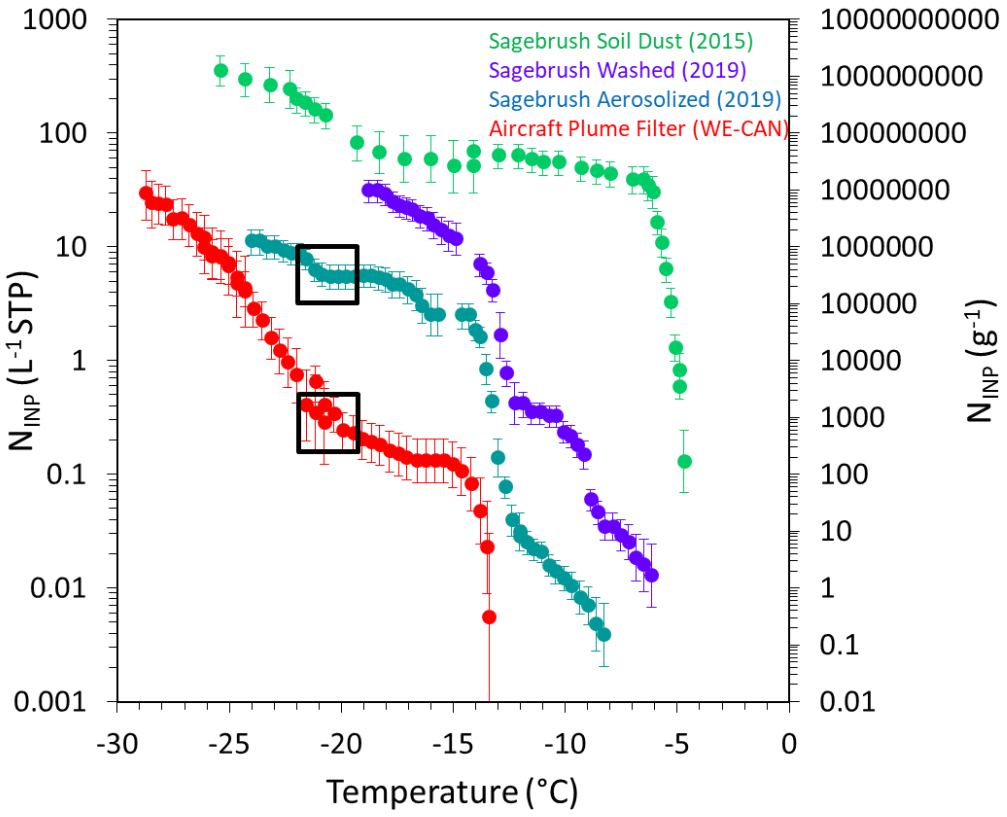

Figure 3.25. INP temperature spectra for the "Jelm" soil dust tested in 2015 (green; right axis), the washed sagebrush tested in 2019 (purple; right axis), the aerosolized sagebrush tested in 2019 (teal; right axis), and the filter collected from the NSF/NCAR C-130 during the South Sugarloaf fire in 2018 (red; left axis). Black boxes highlight a similar inflection point.

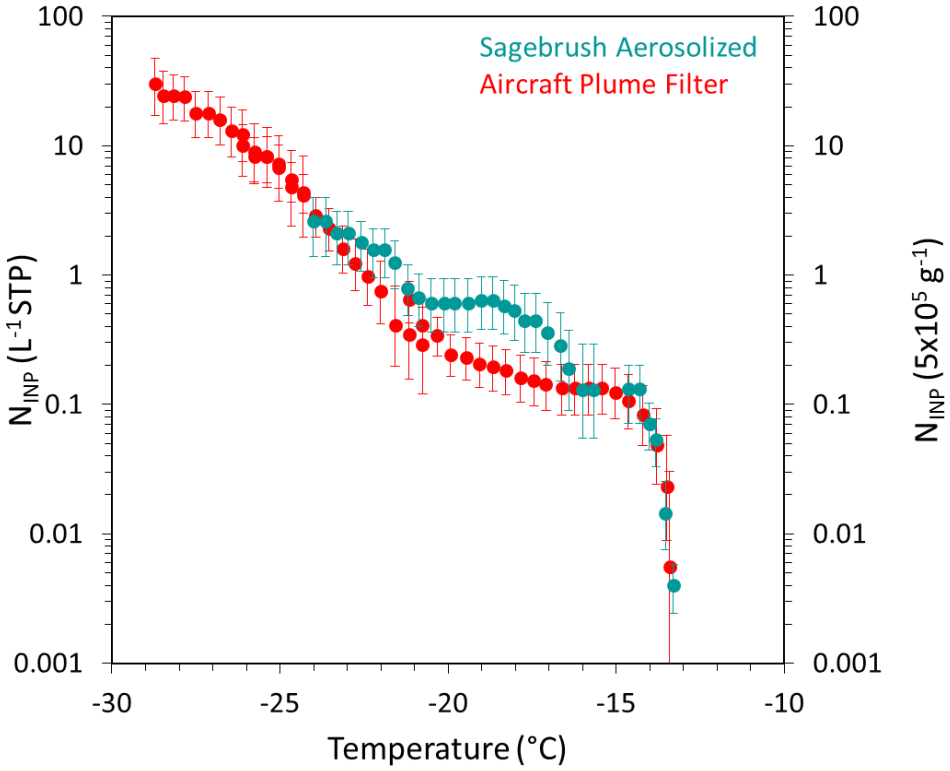

Figure 3.26. INP temperature spectra from “Jelm” aerosolized sagebrush tested in 2019 (teal; right axis) scaled by 500,000 and plotted with the plume filter from the South Sugarloaf fire (red; left axis).

4. Conclusions and Future Work

The WE-CAN campaign sampled many wildfire plumes over the course of July-August 2018. Sixteen research flights were conducted that focused primarily on free-tropospheric measurements. For analysis of INPs, WE-CAN provided a unique opportunity to sample wildfire plumes as almost all prior measurements have been either in the laboratory or at ground level. INP concentrations were made with the online CFDC instrument that measured INPs as single particles in real time on the aircraft and with aerosol filters that collected bulk aerosol samples that were later analyzed by resuspending particles into liquid and testing their freezing spectra with the IS. The results indicate an effect of in-plume versus out-of-plume background air on INP concentrations, but the total increase was fire dependent and generally around an order of magnitude or less. The composition of the smoke INPs were revealed to be primarily organic for all filter suspensions analyzed with peroxide digestion across most of the temperature spectrum, with some filters showing no detectable INPs after this treatment (the Taylor Creek (RF3) and Donnell (RF7) fires). The Taylor Creek (RF3), Donnell (RF7), and Mendocino Complex (RF13) fires also had large contributions from biological presence, as indicated by reduction in INP concentrations after 95 °C heating of particle suspensions tested with the IS. The predominant fuel types for these fires were douglas-fir-madrone-tanoak forest, red fir forest, and chamise chaparral shrubland respectively. The River of Smoke (RF5) and Shellrock (RF11) fire had no reduction in their INP temperature spectrum after heating, indicating minimal contributions from biological INP to the total population. The principal fuel type for the Shellrock fire was Subalpine fir-lodgepole pine-whitebark pine-Engelmann spruce forest. Looking at the predominant fuel type reveals the need for more research on possible reasons

for discrepancy among fire INP emissions, and the many fuels that comprise each of these fires make this problem complex. The refractory black carbon data and modified combustion efficiency calculations can also be used in future research to see if there are any connections with INP concentrations and compare to previous work that link INPs and flaming combustion (Levin et al. 2016). Additionally, the composition of INPs in wildfires is likely influenced by the season of occurrence, as Creamean et al. (2014) found that Asian dust peaks in the U.S. West Coast in spring, which is when the wildfires that McCluskey et al. (2014) sampled occurred.

The most unusual case studied during the WE-CAN campaign was the South Sugarloaf fire in RF15, which had a main fuel type of sagebrush shrubland. The results from the CFDC show a lot of scatter in plume INP concentrations, with some passes over 100 L^{-1}, the highest of the campaign. The plume aerosol filter collected also had a unique slope in the INP temperature spectrum at around -13 °C and looked drastically different from the out-of-plume background filter INP concentrations, despite RF15 having one of the dirtiest backgrounds for the campaign from regional influences of other fires. Testing aerosolized sagebrush shrub clippings for INP properties and comparing to previously tested sagebrush soil dust revealed the likely role of release of INPs (from fire-driven turbulence) contained on the surfaces of sagebrush plants over those from the soil dust. This is based on the INP temperature spectra having distinctive inflection points around -21 °C combined with a unique onset of an INP population that initiates freezing between -13 and -14 °C. Sagebrush fuel has also been shown to have detectable INP activity in Petters et al. (2009) in the FLAME 2 laboratory study. The filter-collected aerosol analyzed with the IS showed a prominent organic INP population as indicated by sensitivity to peroxide digestion at all temperatures, which was observed in other

WE-CAN cases. The higher temporal resolution measured by the CFDC revealed the highest INP concentration passes sampled were generally the ones at the lowest altitudes and with the most aging. The CFDC captured plume passes from the South Sugarloaf fire of over 5000 m above sea level, but the passes with INP concentrations exceeding 100 L^{-1} were all below 4300 m. This speaks to the heterogeneity of this particular plume and its emissions, though future research is needed to investigate any consistent trends in plume INP distributions.

This INP dataset also provided the first attempt at accounting for dilution in plumes by using NEMR analysis for INP concentrations. Although there are a limited number of plume passes along with some uncertainty in the background calculations, most plumes had little variation in NEMR with plume age, which is expected unless there are changes (sources/sinks) to the INP population other than simple dilution. Two exceptions observed are from the Bear Trap (RF9) and South Sugarloaf (RF15) fires that had multiple passes having higher NEMRs that could indicate another process occurring to enhance the INP concentration, such as plant material or dust lofting into the plume downwind of the fire source. Production of INPs is also a possibility in these fires, as tarballs were found in the High Park fire in McCluskey et al. (2014). This question can be answered in the future through analyzing more TEM samples to understand INP composition. Despite these exceptions, the relative consistency of NEMR with enhanced plume age for many of the fires allows for the possibility of INPs from Western U.S. wildfire smoke plumes to be included in future modelling studies and obtain an emission rate via relation to CO emissions.

The plume INP concentrations were normalized in two ways: by total aerosol surface area under 2.5 μm to calculate the surface active site density parameter (n_s) and by expressing

INPs as a fraction of the number concentration of particles above 500 nm in diameter (N_{500}), methods that have been previously used with INP measurements. Normalization by N_{500} allowed for comparison with the wildfires and prescribed burns studied in McCluskey et al. (2014) and revealed similarities of the wildfire plumes measured in WE-CAN and the High Park fire. The previously measured prescribed burn plume had INP values that scattered at the lower end of the WE-CAN plume INP measurements. Calculation of n_s showed that smoke from the Western U.S. is generally not an efficient ice nucleator on a per surface area basis and looks more like clean marine air than a more efficient nucleating particle type such as mineral or soil dust. However, because smoke is a large source of particles, plumes are still able to be a source of INPs that can likely have a regional impact on the INP budget. Some evidence for the impact of smoke INPs came from analyzing whether urban influence affected INP concentrations through calculation of the iso- to n-pentane ratio. There was no correlation found between this ratio, which is higher with greater urban influence, and INP number concentrations. Therefore, it can be predicted that there is little contribution of urban airmasses on INPs over smoke (with this particular tracer), and likewise this suggests that urban emissions do not exert a regional influence.

The work presented herein focused on analyzing several wildfire plumes, but the WE-CAN dataset included many flights that were focused on the interaction between smoke and clouds. As mentioned in Section 2, the CFDC sampled off a counterflow virtual impactor (CVI) inlet to measure cloud droplet residuals that can initiate ice formation. Several cumulus cloud fields were sampled with the best cases from research flights 6, 10, and 12, while research flight 14 sampled a marine stratocumulus deck over coastal California. Additionally, aerosol filters

were collected above and below many of these cloud fields, and cloud water collected from RF14 was stored frozen for later immersion freezing analysis with the IS. Initial findings in RF14 (Figure 4.1) point to homogeneity in the airmasses sampled from similarities in INP concentrations above, below, and in the cloud. Additionally, preliminary TEM data from in and out of clouds support the large organic INP population found during WE-CAN and will be used in future analysis.

Other future work includes DNA extraction and sequencing of several smoke aerosol filter suspensions (total aerosol—not just INPs) to have greater insight into the biological material that may potentially serve as INPs (Figure 4.2). These results could differentiate between sources (e.g. soil versus plant-derived) and reveal if any are known ice nucleating types. There is still more work to be done with the fire dataset, especially to see if any further connections can be drawn from the extensive list of fuels that comprise the fires. There was also cleaner free tropospheric air that was measured in RF16 near Boise that may enhance understanding of the generalized Western U.S. background CO levels during summer 2018, but likely more research will be needed to fully characterize the free-tropospheric background INP levels. Additionally, there is a potential of using some descents into Boise that would provide more smoke-urban interaction data.

Overall, this work shows that smoke particles with primarily organic compositions that were emitted from the fires studied during WE-CAN for a variety of different fuel types serve as free-tropospheric INPs that may later play a role in cloud formation and affect the climate. These results indicate some variability in INP concentrations among fires but low ice nucleation efficiency in smoke after normalization by surface area. More research is especially needed on

connecting fuels to INP emissions in free tropospheric plumes and pinpointing the sources of what is lofted into the plume, as suggested by the role of INPs from the sagebrush plant being lofted in the plume. Distinguishing between a plume and its background air has proved to be a challenging issue from the often "dirty" background from other plume remnants and is generally fire-specific, but there is evidence for increases in plume for most filters analyzed. Future TEM and DNA work may elucidate the nature of the organic and biological particles that were largely present and broaden the understanding of smoke INPs. Since this campaign provided the first free-tropospheric INP measurements from wildfires, more data will be needed to solidify the conclusions here and verify the generally constant trends in NEMR with plume age for implementation in models. However, this study shows that smoke INPs are found in the free troposphere and away from their emissions source and therefore are relevant in a future climate with increased frequency of wildfires.

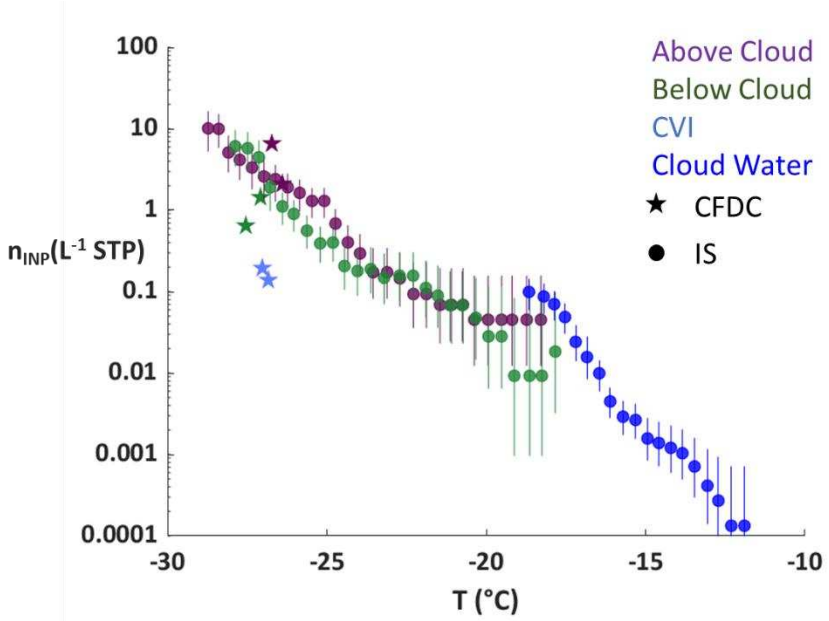

Figure 4.1. Example of an INP temperature spectra for the marine stratocumulus flight in RF14, with the stars representing CFDC data and circles representing IS data.

Figure 4.2. Initial PCR Amplification Results for 500 base pairs for WE-CAN smoke samples (G1,H1,A2) and field blank (B2).

References

Abatzoglou, J. T., & Williams, A. P. (2016). Impact of anthropogenic climate change on wildfire across western US forests. *Proceedings of the National Academy of Sciences*, *113*(42), 11770–11775. https://doi.org/10.1073/pnas.1607171113

Bi, K., McMeeking, G. R., Ding, D. P., Levin, E. J. T., DeMott, P. J., Zhao, D. L., … Chen, P. (2019). Measurements of Ice Nucleating Particles in Beijing, China. *Journal of Geophysical Research: Atmospheres*, *124*(14), 8065–8075. https://doi.org/10.1029/2019JD030609

Bowers, R. M., McLetchie, S., Knight, R., & Fierer, N. (2011). Spatial variability in airborne bacterial communities across land-use types and their relationship to the bacterial communities of potential source environments. *The ISME Journal*, *5*(4), 601–612. https://doi.org/10.1038/ismej.2010.167

Creamean, J. M., Spackman, J. R., Davis, S. M., & White, A. B. (2014). Climatology of long-range transported Asian dust along the West Coast of the United States: Climatology of Asian Dust in the U.S. *Journal of Geophysical Research: Atmospheres*, *119*(21), 12,171-12,185. https://doi.org/10.1002/2014JD021694

de Boer, G., Morrison, H., Shupe, M. D., & Hildner, R. (2011). Evidence of liquid dependent ice nucleation in high-latitude stratiform clouds from surface remote sensors. *Geophysical Research Letters*, *38*(1), n/a-n/a. https://doi.org/10.1029/2010GL046016

DeMott, P. J., (1995) Quantitative descriptions of ice formation mechanisms of silver iodide–type aerosols. *Atmos. Res.,* 38, 63–99, doi:10.1016/0169-8095(94)00088-U

DeMott, P. J., Prenni, A. J., Liu, X., Kreidenweis, S. M., Petters, M. D., Twohy, C. H., … Rogers, D. C. (2010). Predicting global atmospheric ice nuclei distributions and their impacts on climate. *Proceedings of the National Academy of Sciences*, *107*(25), 11217–11222. https://doi.org/10.1073/pnas.0910818107

DeMott, P. J., Prenni, A. J., McMeeking, G. R., Sullivan, R. C., Petters, M. D., Tobo, Y., … Kreidenweis, S. M. (2015). Integrating laboratory and field data to quantify the immersion freezing ice nucleation activity of mineral dust particles. *Atmospheric Chemistry and Physics*, *15*(1), 393–409. https://doi.org/10.5194/acp-15-393-2015

DeMott, Paul J., Hill, T. C. J., Petters, M. D., Bertram, A. K., Tobo, Y., Mason, R. H., … Kreidenweis, S. M. (2017). Comparative measurements of ambient atmospheric concentrations of ice nucleating particles using multiple immersion freezing methods and a continuous flow diffusion chamber. *Atmospheric Chemistry and Physics*, *17*(18), 11227–11245. https://doi.org/10.5194/acp-17-11227-2017

DeMott, Paul J., Möhler, O., Cziczo, D. J., Hiranuma, N., Petters, M. D., Petters, S. S., … Zenker, J. (2018). The Fifth International Workshop on Ice Nucleation phase 2 (FIN-02): Laboratory intercomparison of ice nucleation measurements. *Atmospheric Measurement Techniques*, *11*(11), 6231–6257. https://doi.org/10.5194/amt-11-6231-2018

Garcia, E., Hill, T. C. J., Prenni, A. J., DeMott, P. J., Franc, G. D., & Kreidenweis, S. M. (2012). Biogenic ice nuclei in boundary layer air over two U.S. High Plains agricultural regions. *Journal of Geophysical Research: Atmospheres*, *117*(D18), n/a-n/a. https://doi.org/10.1029/2012JD018343

Garofalo, L. A., Pothier, M. A., Levin, E. J. T., Campos, T., Kreidenweis, S. M., & Farmer, D. K. (2019). Emission and Evolution of Submicron Organic Aerosol in Smoke from Wildfires in the Western United States. *ACS Earth and Space Chemistry*, *3*(7), 1237–1247. https://doi.org/10.1021/acsearthspacechem.9b00125

Grawe, S., Augustin-Bauditz, S., Hartmann, S., Hellner, L., Pettersson, J. B. C., Prager, A., … Wex, H. (2016). The immersion freezing behavior of ash particles from wood and brown coal burning. *Atmospheric Chemistry and Physics*, *16*(21), 13911–13928. https://doi.org/10.5194/acp-16-13911-2016

Hill, T. C. J., DeMott, P. J., Conen, F., & Möhler, O. (2018). Impacts of Bioaerosols on Atmospheric Ice Nucleation Processes. In A.-M. Delort & P. Amato (Eds.), *Microbiology of Aerosols* (1st ed., pp. 197–219). John Wiley & Sons.

Hill, Thomas C. J., Moffett, B. F., DeMott, P. J., Georgakopoulos, D. G., Stump, W. L., & Franc, G. D. (2014). Measurement of Ice Nucleation-Active Bacteria on Plants and in Precipitation by Quantitative PCR. *Applied and Environmental Microbiology*, *80*(4), 1256–1267. https://doi.org/10.1128/AEM.02967-13

Hill, Tom C. J., DeMott, P. J., Tobo, Y., Fröhlich-Nowoisky, J., Moffett, B. F., Franc, G. D., & Kreidenweis, S. M. (2016). Sources of organic ice nucleating particles in soils. *Atmospheric Chemistry and Physics*, *16*(11), 7195–7211. https://doi.org/10.5194/acp-16-7195-2016

Kanji, Z. A., Ladino, L. A., Wex, H., Boose, Y., Burkert-Kohn, M., Cziczo, D. J., & Krämer, M. (2017). Overview of Ice Nucleating Particles. *Meteorological Monographs*, *58*, 1.1-1.33. https://doi.org/10.1175/AMSMONOGRAPHS-D-16-0006.1

Krishnamoorthy, K., & Lee, M. (2013). New approximate confidence intervals for the difference between two Poisson means and comparison. *Journal of Statistical Computation and Simulation*, *83*(12), 2232–2243. https://doi.org/10.1080/00949655.2012.686616

Kupc, A., Williamson, C., Wagner, N. L., Richardson, M., & Brock, C. A. (2018). Modification, calibration, and performance of the Ultra-High Sensitivity Aerosol Spectrometer for particle size

distribution and volatility measurements during the Atmospheric Tomography Mission (ATom) airborne campaign. *Atmospheric Measurement Techniques*, *11*(1), 369–383. https://doi.org/10.5194/amt-11-369-2018

Levin, E. J. T., McMeeking, G. R., DeMott, P. J., McCluskey, C. S., Carrico, C. M., Nakao, S., … Kreidenweis, S. M. (2016). Ice-nucleating particle emissions from biomass combustion and the potential importance of soot aerosol: Ice Nuclei From Biomass Combustion. *Journal of Geophysical Research: Atmospheres*, *121*(10), 5888–5903. https://doi.org/10.1002/2016JD024879

Lohmann, U. (2002). A glaciation indirect aerosol effect caused by soot aerosols. *Geophysical Research Letters*, *29*(4), 1052. https://doi.org/10.1029/2001GL014357

Lohmann, Ulrike, & Gasparini, B. (2017). A cirrus cloud climate dial? *Science*, *357*(6348), 248–249. https://doi.org/10.1126/science.aan3325

McClure, C. D., & Jaffe, D. A. (2018). US particulate matter air quality improves except in wildfire-prone areas. *Proceedings of the National Academy of Sciences*, *115*(31), 7901–7906. https://doi.org/10.1073/pnas.1804353115

McCluskey, C. S., DeMott, P. J., Prenni, A. J., Levin, E. J. T., McMeeking, G. R., Sullivan, A. P., … Kreidenweis, S. M. (2014). Characteristics of atmospheric ice nucleating particles associated with biomass burning in the US: Prescribed burns and wildfires: Biomass burning ice nucleating particles. *Journal of Geophysical Research: Atmospheres*, *119*(17), 10458–10470. https://doi.org/10.1002/2014JD021980

McCluskey, C. S., Ovadnevaite, J., Rinaldi, M., Atkinson, J., Belosi, F., Ceburnis, D., … DeMott, P. J. (2018). Marine and Terrestrial Organic Ice-Nucleating Particles in Pristine Marine to Continentally Influenced Northeast Atlantic Air Masses. *Journal of Geophysical Research: Atmospheres*, *123*(11), 6196–6212. https://doi.org/10.1029/2017JD028033

Mülmenstädt, J., Sourdeval, O., Delanoë, J., & Quaas, J. (2015). Frequency of occurrence of rain from liquid-, mixed-, and ice-phase clouds derived from A-Train satellite retrievals: RAIN FROM LIQUID- AND ICE-PHASE CLOUDS. *Geophysical Research Letters*, *42*(15), 6502–6509. https://doi.org/10.1002/2015GL064604

Murray, B. J., O'Sullivan, D., Atkinson, J. D., & Webb, M. E. (2012). Ice nucleation by particles immersed in supercooled cloud droplets. *Chemical Society Reviews*, *41*(19), 6519. https://doi.org/10.1039/c2cs35200a

Niemand, M., Möhler, O., Vogel, B., Vogel, H., Hoose, C., Connolly, P., … Leisner, T. (2012). A Particle-Surface-Area-Based Parameterization of Immersion Freezing on Desert Dust Particles. *Journal of the Atmospheric Sciences*, *69*(10), 3077–3092. https://doi.org/10.1175/JAS-D-11-0249.1

Petters, M. D., Parsons, M. T., Prenni, A. J., DeMott, P. J., Kreidenweis, S. M., Carrico, C. M., … Moosmüller, H. (2009). Ice nuclei emissions from biomass burning. *Journal of Geophysical Research*, *114*(D7), D07209. https://doi.org/10.1029/2008JD011532

Petty, G. W. (2006). *A first course in atmospheric radiation* (2nd ed). Madison, Wis: Sundog Pub.

Pratt, K. A., DeMott, P. J., French, J. R., Wang, Z., Westphal, D. L., Heymsfield, A. J., … Prather, K. A. (2009). In situ detection of biological particles in cloud ice-crystals. *Nature Geoscience*, *2*(6), 398–401. https://doi.org/10.1038/ngeo521

Prenni, A. J., DeMott, P. J., Sullivan, A. P., Sullivan, R. C., Kreidenweis, S. M., & Rogers, D. C. (2012). Biomass burning as a potential source for atmospheric ice nuclei: Western wildfires and prescribed burns. *Geophysical Research Letters*, *39*(11), n/a-n/a. https://doi.org/10.1029/2012GL051915

Price, H. C., Baustian, K. J., McQuaid, J. B., Blyth, A., Bower, K. N., Choularton, T., … Murray, B. J. (2018). Atmospheric Ice-Nucleating Particles in the Dusty Tropical Atlantic. *Journal of Geophysical Research: Atmospheres*, *123*(4), 2175–2193. https://doi.org/10.1002/2017JD027560

Rogers, D. C. (1988). Development of a continuous flow thermal gradient diffusion chamber for ice nucleation studies. *Atmospheric Research*, *22*(2), 149–181. https://doi.org/10.1016/0169-8095(88)90005-1

Rogers, D. C., DeMott, P. J., & Kreidenweis, S. M. (2001). Airborne measurements of tropospheric ice-nucleating aerosol particles in the Arctic spring. *Journal of Geophysical Research: Atmospheres*, *106*(D14), 15053–15063. https://doi.org/10.1029/2000JD900790

Schiebel, T. (2017). *Ice Nucleation Activity of Soil Dust Aerosols*. Karlsruhe Institute of Technology, Karlsruhe, Germany.

Schill, G. P., Jathar, S. H., Kodros, J. K., Levin, E. J. T., Galang, A. M., Friedman, B., … DeMott, P. J. (2016). Ice-nucleating particle emissions from photochemically aged diesel and biodiesel exhaust. *Geophysical Research Letters*, *43*(10), 5524–5531. https://doi.org/10.1002/2016GL069529

Seinfeld, J. H., & Pandis, S. N. (2016). *Atmospheric chemistry and physics: From air pollution to climate change* (Third edition). Hoboken, New Jersey: John Wiley & Sons.

Simpson, I. J., Akagi, S. K., Barletta, B., Blake, N. J., Choi, Y., Diskin, G. S., … Blake, D. R. (2011). Boreal forest fire emissions in fresh Canadian smoke plumes: C_1-C_{10} volatile organic compounds (VOCs), CO_2, CO, NO_2, NO, HCN and CH_3CN. *Atmospheric Chemistry and Physics*, *11*(13), 6445–6463. https://doi.org/10.5194/acp-11-6445-2011

Suski, K. J., Hill, T. C. J., Levin, E. J. T., Miller, A., DeMott, P. J., & Kreidenweis, S. M. (2018). Agricultural harvesting emissions of ice-nucleating particles. *Atmospheric Chemistry and Physics*, *18*(18), 13755–13771. https://doi.org/10.5194/acp-18-13755-2018

Thompson, C. R., Hueber, J., & Helmig, D. (2014). Influence of oil and gas emissions on ambient atmospheric non-methane hydrocarbons in residential areas of Northeastern Colorado. *Elementa: Science of the Anthropocene*, *2*, 000035. https://doi.org/10.12952/journal.elementa.000035

Tobo, Y., DeMott, P. J., Hill, T. C. J., Prenni, A. J., Swoboda-Colberg, N. G., Franc, G. D., & Kreidenweis, S. M. (2014). Organic matter matters for ice nuclei of agricultural soil origin. *Atmospheric Chemistry and Physics*, *14*(16), 8521–8531. https://doi.org/10.5194/acp-14-8521-2014

Ullrich, R., Hoose, C., Möhler, O., Niemand, M., Wagner, R., Höhler, K., … Leisner, T. (2017). A New Ice Nucleation Active Site Parameterization for Desert Dust and Soot. *Journal of the Atmospheric Sciences*, *74*(3), 699–717. https://doi.org/10.1175/JAS-D-16-0074.1

Umo, N. S., Murray, B. J., Baeza-Romero, M. T., Jones, J. M., Lea-Langton, A. R., Malkin, T. L., … Williams, A. (2015). Ice nucleation by combustion ash particles at conditions relevant to mixed-phase clouds. *Atmospheric Chemistry and Physics*, *15*(9), 5195–5210. https://doi.org/10.5194/acp-15-5195-2015

Vali, G. (1971). Quantitative Evaluation of Experimental Results and the Heterogeneous Freezing Nucleation of Supercooled Liquids, *Journal of the Atmospheric Sciences*, 28, 402-209, 10.1175/1520-0469(1971)028<0402:QEOERA>2.0.CO;2, 1971.

Vali, G., DeMott, P. J., Möhler, O., & Whale, T. F. (2015). Technical Note: A proposal for ice nucleation terminology. *Atmospheric Chemistry and Physics*, *15*(18), 10263–10270. https://doi.org/10.5194/acp-15-10263-2015

Ward, D. E., & Radke, L. F. (1993). Emissions Measurements from Vegetation Fires: A Comparative Evaluation of Methods and Results. 24.

WE-CAN Field Catalog | NCAR EOL. (n.d.). Retrieved September 18, 2019, from http://catalog.eol.ucar.edu/we-can

Westerling, A. L. (2016). Increasing western US forest wildfire activity: Sensitivity to changes in the timing of spring. *Philosophical Transactions of the Royal Society B: Biological Sciences*, *371*(1696), 20150178. https://doi.org/10.1098/rstb.2015.0178

Williamson, G. J., Price, O. F., Henderson, S. B., & Bowman, D. M. J. S. (2013). Satellite-based comparison of fire intensity and smoke plumes from prescribed fires and wildfires in south-

eastern Australia. *International Journal of Wildland Fire*, *22*(2), 121. https://doi.org/10.1071/WF11165

Yokelson, R. J., Andreae, M. O., & Akagi, S. K. (2013). Pitfalls with the use of enhancement ratios or normalized excess mixing ratios measured in plumes to characterize pollution sources and aging. *Atmospheric Measurement Techniques*, *6*(8), 2155–2158. https://doi.org/10.5194/amt-6-2155-2013